



**Oxic methane production in shallow productive lakes:
linking field and in vitro experimental evidence**

Sofía Baliña^{1*}, María Laura Sánchez¹, Mina Bizic², Danny Ionescu², Shoji D. Thottathil³, María Carolina Bernal¹, Angela Juárez⁴, Hans-Peter Grossart^{5,6}, Paul A. del Giorgio⁷

¹Laboratorio de Limnología, Departamento de Ecología, Genética y Evolución, Facultad de Ciencias Exactas y Naturales, Universidad de Buenos Aires, Instituto de Ecología, Genética y Evolución de Buenos Aires (IEGEBA - CONICET/UBA), Ciudad Autónoma de Buenos Aires, Argentina

²Chair of Environmental Microbiomics, Technische Universität Berlin, Berlin, Germany

³Department of Environmental Science and Engineering, SRM University AP, Amaravati, Andhra Pradesh 522 502, India.

⁴Universidad de Buenos Aires, Facultad de Ciencias Exactas y Naturales, Departamento de Biodiversidad y Biología Experimental and CONICET-Universidad de Buenos Aires, Instituto de Biodiversidad y Biología Experimental y Aplicada (IBBEA), Buenos Aires, Argentina.

⁵Leibniz Institute of Freshwater Ecology and Inland Fisheries (IGB), Alte Fischerhütte 2, D-16775 Stechlin, Germany.

⁶Institute of Biochemistry and Biology, Potsdam University, Maulbeerallee 2, D-16775 Stechlin, Germany

⁷Département des Sciences Biologiques, Université du Québec à Montréal, Montréal, Québec, Canada

*Corresponding author: sofiabalinia@gmail.com

Email addresses, in the corresponding order: sofiabalinia@gmail.com, laurasanchez@ege.fcen.uba.ar, mina.bizic@tu-berlin.de, ionescu@tu-berlin.de, shoji.thottathil@gmail.com, carobernal90@gmail.com, juarez.ab@gmail.com, hgrossart@igb-berlin.de, del_giorgio.paul@uqam.ca

Peer review status: This is a non-peer-reviewed preprint submitted to EarthArXiv

**Oxic methane production in shallow productive lakes:
linking field and in vitro experimental evidence**

Sofía Baliña^{1*}, María Laura Sánchez¹, Mina Bizic², Danny Ionescu², Shoji D. Thottathil³, María Carolina Bernal¹, Angela Juárez⁴, Hans-Peter Grossart^{5,6}, Paul A. del Giorgio⁷

¹Laboratorio de Limnología, Departamento de Ecología, Genética y Evolución, Facultad de Ciencias Exactas y Naturales, Universidad de Buenos Aires, Instituto de Ecología, Genética y Evolución de Buenos Aires (IEGEBA - CONICET/UBA), Ciudad Autónoma de Buenos Aires, Argentina

²Chair of Environmental Microbiomics, Technische Universität Berlin, Berlin, Germany

³Department of Environmental Science and Engineering, SRM University AP, Amaravati, Andhra Pradesh 522 502, India.

⁴Universidad de Buenos Aires, Facultad de Ciencias Exactas y Naturales, Departamento de Biodiversidad y Biología Experimental and CONICET-Universidad de Buenos Aires, Instituto de Biodiversidad y Biología Experimental y Aplicada (IBBEA), Buenos Aires, Argentina.

⁵Leibniz Institute of Freshwater Ecology and Inland Fisheries (IGB), Alte Fischerhütte 2, D-16775 Stechlin, Germany.

⁶Institute of Biochemistry and Biology, Potsdam University, Maulbeerallee 2, D-16775 Stechlin, Germany

⁷Département des Sciences Biologiques, Université du Québec à Montréal, Montréal, Québec, Canadá

*Corresponding author: sofiabalinia@gmail.com

Abstract

Whereas the occurrence of oxic methane (CH₄) production (OMP) in the oxygenated water column of lakes is widely accepted, its mechanisms, isotopic signature, and contribution to total CH₄ emissions remain uncertain. Evidence suggests that phytoplankton produces CH₄, but it is unclear to what extent this pathway contributes to ecosystem OMP rates. Shallow lakes are often productive and feature high phytoplankton biomass, implying that OMP rates could be high and contribute substantially to CH₄ emissions. Here we present results of an extensive field mesocosm study carried out in three shallow and productive lakes in the Pampean Plain (Argentina), designed to assess ambient OMP dynamics. We combined this with in vitro experiments to quantify the potential CH₄ production by dominant phytoplankton strains from these systems. We demonstrate that OMP occurred in all lakes, albeit at rates that were lower than expected given their productivity; all phytoplankton strains produced CH₄, yet our results suggest that phytoplankton CH₄ production contributed up to 14% to OMP rates, implying that other pathways dominate the observed OMP. The contribution of OMP to lake CH₄ diffusive emissions was low for all lakes, suggesting that sediment CH₄ production is the main source for CH₄ emissions in these ecosystems.

Introduction

The traditional understanding of methane (CH_4) cycling in aquatic ecosystems considers that biological CH_4 is solely produced under anoxic conditions by methanogenic archaea¹. However, the frequent supersaturation of CH_4 that is observed in oxic surface waters of aquatic ecosystems cannot be explained solely by transport of CH_4 from anoxic sediments and deeper water layers^{2–5}, generating what has been termed the “methane paradox”. Over the last decade there have been numerous reports of CH_4 production in the oxic water column of aquatic ecosystems through various mechanisms, both under oxic and anoxic conditions^{6,7}. These newly identified sources of CH_4 are referred to as Oxidic Methane Production (OMP), considering that they occur in the oxygenated portion of the water column but not necessarily under oxic conditions⁸. Collectively, these studies have demonstrated that there is no actual paradox but rather that the pathways of aquatic CH_4 production are more diverse and complex than previously thought^{5,9}.

There are several known metabolic pathways, in addition to archaeal methanogenesis, which produce CH_4 . There are reports of aerobic production of CH_4 as a byproduct of methyl-phosphonates (MPn) decomposition by aerobic heterotrophs in marine^{2,10,11} and freshwater environments^{12–14}. Similarly, aerobic demethylation of dimethyl sulfoniopropionate (DMSP) has been reported to produce methanethiol in marine waters, with the subsequent release of CH_4 ³. Aerobic metabolism of methylamine (MeA) has been also reported as a source of methane in lakes^{6,15} and it was even been hypothesized that all living cells can produce CH_4 by a common mechanism triggered by free iron and reactive oxygen species (ROS)¹⁶. There is also growing evidence for a coupling between OMP and phytoplankton^{17,18}. Grossart et al. (2011)^{4,19} detected methanogenic archaea in oxic waters of a lake in Germany, which were attached to phytoplankton and possibly living in micro-anoxic niches associated with algal cells. Moreover, several reports indicated a link between OMP and photosynthesis at an ecosystem scale^{20–23}. In this regard, it has been experimentally shown that various phytoplanktonic groups including diatoms²¹, cyanobacteria^{24,25}, haptophytes, and marine microalgal species^{25–27} produce CH_4 , and that the rate of production is somehow linked to temperature and light exposure^{24,28}. There appear to be multiple coexisting OMP pathways in freshwaters, and these probably vary in relative importance among aquatic ecosystems, along trophic and other environmental gradients^{7,29,30}. Regardless of the mechanisms behind OMP, there is still much uncertainty as to the magnitude of the rates of OMP at the ecosystem scale and the contribution of these pathways to freshwater CH_4 emissions. There have been various attempts to address these questions, based on whole-lake^{22,29,31,32} or mesocosm²⁰ mass balances, and also based on experimental incubations of lake water^{4,5,7,29,31}. Reported ecosystem OMP rates vary from $0.01 \mu\text{M day}^{-1}$ up to $0.52 \mu\text{M day}^{-1}$ ^{15,20,22,29,31,32}. The handful of studies that have quantified the contribution of OMP to total lake CH_4 production or to total lake CH_4 emissions in the surface mixed layer of stratified lakes have reported a wide range of values, from $< 5\%$ to up to $\sim 80\%$ ^{29,31–33}, that also seem to depend on core morphometric features of freshwater ecosystems, which the contribution of OMP increasing with decreasing sediment area to volume

ratio^{31,32}. Hence, the factors that regulate the rates of OMP and the contribution of these pathways to total ecosystem CH₄ emissions are still not well understood.

OMP pathways also contribute to the isotopic CH₄ balances in the water column, and therefore to the processes that are inferred from these. The isotopic signature of ambient and source $\delta^{13}\text{C-CH}_4$ have been used to assess the extent of CH₄ oxidation in the water column, where the source has traditionally been assumed to be one of the two main anoxic methanogenic pathways which typically yield very depleted CH₄ (-65 to -110³⁴). There is increasing evidence that $\delta^{13}\text{C-CH}_4$ generated by the various OMP pathways is highly variable but generally more enriched than $\delta^{13}\text{C-CH}_4$ generated by archaeal methanogenesis^{25,30,32,35}. Since OMP pathways generate enriched $\delta^{13}\text{C-CH}_4$ that overlaps with the signature of partially oxidized methanogenic CH₄, the existence of OMP complexifies the CH₄ isotopic mass balance in surface waters, and it is therefore important to better characterize the $\delta^{13}\text{C-CH}_4$ associated to OMP pathways.

OMP rates and their contribution to ecosystem CH₄ emissions have been mostly explored in oligo- to mesotrophic lakes that tend to stratify, and there has been very little work done on shallow polymictic lakes²³. These lakes tend to be productive and develop high phytoplankton biomass³⁶, for this reason and it could be expected that the rates of OMP might be high relative to other lakes, yet the contribution of OMP to total CH₄ diffusive fluxes may still be modest given the importance of sediments in these shallow systems. In addition, the phytoplankton communities of shallow lakes may be dominated by entirely different taxa³⁷, and these contrasts in community composition could potentially lead to differences in ambient OMP and in the potential values of $\delta^{13}\text{C-CH}_4$ derived from OMP as well. To test these contrasting hypotheses, we present an integrative study that combines ecosystem, mesocosm and in vitro approaches to assess the magnitude and the ecosystem-level contribution of OMP, as well as the potential contribution of phytoplankton to this process, in three shallow lakes with different abundance and composition of phytoplanktonic communities. In situ mesocosm experiments were carried out in each lake to quantify OMP rates and to assess the potential values of $\delta^{13}\text{C-CH}_4$ derived from OMP. In addition, sampling of the lakes allowed extrapolating the mesocosm results to determine the contribution of OMP to whole lake CH₄ emissions. Finally, phytoplankton strains were isolated from each one of these lakes and used to carry out in vitro experiments to assess their potential CH₄ production rates, which were subsequently used to infer the potential contribution of phytoplankton to ambient OMP in these lakes.

Methods

1. Study area

Field experiments were carried out in three lakes previously studied^{36,38} in the Pampean Plain of Buenos Aires, Argentina (35°32'–36°48'S; 57°47'–58°07'W), *La Salada* (SA), *El Burro* (BU) and *La Segunda* (SG) (Fig. S1). These lakes are shallow, polymictic and naturally eutrophic or hypereutrophic. SA and BU are very turbid due to high algal biomass, with no presence of submerged macrophytes; whereas SG has a much lower algal biomass and water turbidity, with submerged macrophytes development, and these lakes

also tend to present different phytoplanktonic community compositions³⁶. A detailed description of the Pampean Plain region is presented in Baliña *et al.* (2022b)³⁶.

2. Experimental design

Field experiments were carried out in the 2021 austral summer, between 25th and 28th of January in SA; 29th of January and 2nd of February in SG; 2nd and 6th of February in BU. In each lake, three (SA) or four (SG, BU) mesocosms were deployed (Fig. 1A, Fig. S2). Mesocosms were built with the same transparent polycarbonate sheets as in Bogard *et al.* (2014)²⁰, which allows the passage of photosynthetically active radiation (PAR) but restricts the diffusion of gasses (Suppl. Inf. 1). Mesocosms were 0.8 m deep, 1 m wide, and closed at the bottom to exclude sediment CH₄ input. They had a floating device and a protective rim to prevent water from the lake entering the enclosure, and they were anchored to the sediment to prevent them from moving. The average depth of the lakes at the time of the experiments was 1.2 m, 0.9 m and 0.9 m for SA, SG and BU, respectively. Prior to the onset of the experiments, the enclosures were filled with water from 0.2 m below the surface of each lake using a submersible pump (Proactive Pump II, Waterspout 2, Proactive Environmental Products®) with a velocity of 15.12 liters min⁻¹. The water was run through a shower head device to equilibrate the dissolved gases with the atmosphere. The latter was done to lower the initial CH₄ baseline (while retaining saturation of O₂ and CO₂) and therefore to facilitate the detection of changes in CH₄ concentration within the mesocosms during the experimental period. In addition, water was filtered through a 55 µm pore size net to exclude large zooplankton that could graze on phytoplankton. After filling the mesocosms, high frequency oxygen (O₂) and temperature (T) sensors (miniDO₂T, Precision Measurement Engineering, Inc.®) were deployed inside each mesocosm as well as in the lake, in all cases at 0.4 m depth. These devices measured T (°C), O₂ (mg L⁻¹), and O₂ saturation (%) every 5 minutes for the entire duration of the experiment. Note that in the clear lake submerged macrophytes were not included inside the mesocosms, since our study primarily focused on exploring CH₄ production by the planktonic communities. The length of the experimental deployment varied slightly among lakes due to logistic considerations, including constraints imposed by COVID restrictions. To ensure consistency, here we present the results from the initial 100-hour deployment for all experiments. The detailed sampling design is shown in Table S1 (Table S1).

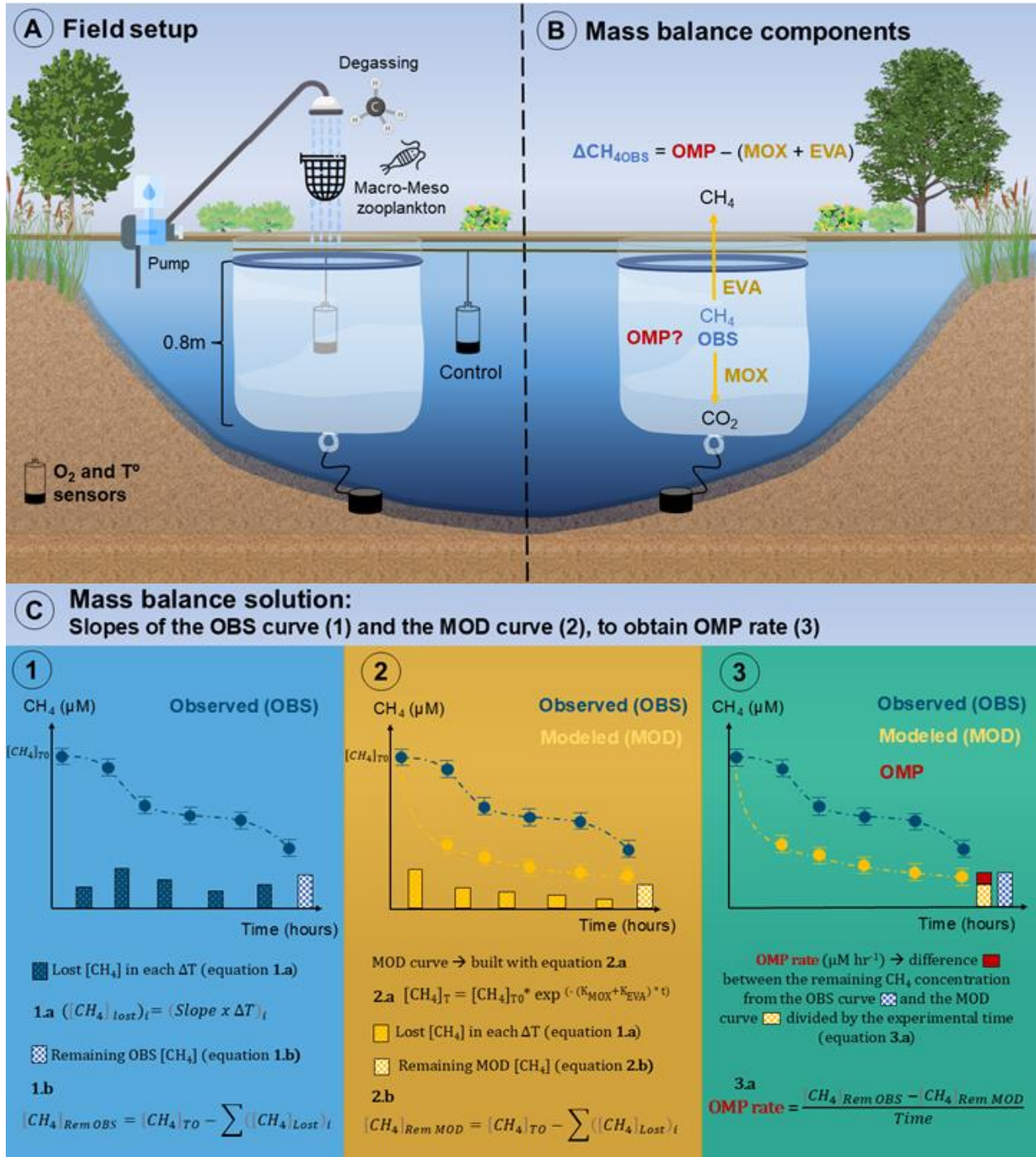


Figure 1. Overview of mesocosm field experiments and mass balance approach to estimate OMP rates. A) Illustration of the field setup, indicating how the mesocosms were filled and where the O_2 / T sensors were located; B) Mass balance components: the change in CH_4 dissolved inside the enclosures between two consecutive time points (ΔCH_{4OBS}) is the result of the potential CH_4 produced through OMP (OMP) minus the CH_4 oxidized (MOX) and the CH_4 lost to the atmosphere through diffusion (EVA); C) Mass balance solution: the modeled curve predicts the expected CH_4 concentration in the mesocosms considering loss

of CH₄ through oxidation (MOX) and evasion (EVA), and compares this to the observed curve (OBS). If the observed curve is higher than the modelled one, this implies OMP, because the mesocosms are isolated from the sediment. The steps for this approach are: 1) estimating the remaining CH₄ concentration at the end of the experiment by multiplying the slope of the CH₄ concentration vs time of each time segment, by the respective delta time (eq. 1.a), to calculate the difference between the initial CH₄ mass and the total change in CH₄ mass over the course of the experiment (eq. 1.b); 2) obtaining the expected CH₄ concentration in the mesocosms as the result of loss of CH₄ by oxidation and diffusion was modeled using eq. 2.a. The remaining modeled CH₄ concentration at the end of the experiment was obtained as described before, using eq. 1.a to obtain the change in CH₄ in each time segment, and equation 2.b to obtain the final CH₄ concentration; 3) subtraction of the remaining modeled CH₄ concentration from the remaining observed CH₄ concentration, divided by the time course of the experiment (eq. 3a). A detailed description of the mass balance solution can be found in section 6. *Tree and bush symbols from Dylan Taillie and Jane Hawkey, respectively, and emergent macrophyte symbols from Tracey Saxby, Integration and Application Network, University of Maryland Center for Environmental Science.*

3. Limnological characterization

In both mesocosms and lakes, T and O₂ high-frequency sensors were supplemented with water T and O₂ profiles measured at 10 cm intervals. An irradiance profile was carried out in the mesocosms and the lakes, to assess the vertical attenuation coefficient for photosynthetically active radiation (K_{dpar}). Additionally, pH, turbidity, total suspended solids (TSS), total phosphorus (TP), total nitrogen (TN), dissolved organic carbon (DOC), dissolved inorganic carbon (DIC), chlorophyll *a* (Chl*a*), and phytoplankton abundance and composition were analyzed both in the mesocosms and the lakes³⁶. Archaeal and bacterial community compositions were analyzed as described in Suppl. Inf. 2. Ecosystem metabolism was calculated as specified in Suppl. Inf. 3. Atmospheric pressure, humidity and wind speed were recorded using a Kestrel (Kestrel, 4000 Pocket Weather Tracker ®, Nielsen-Kellerman®).

4. Greenhouse gas analysis

4.1 Dissolved gas concentration and Isotopic values

Dissolved CH₄ and carbon dioxide (CO₂) concentration in the water were obtained by means of the headspace equilibration method³⁶. Headspace samples were analyzed using a cavity ringdown spectrometer (Picarro G2201-i) to obtain the partial pressures (ppmv) and ¹³C values of CH₄ and CO₂. The original ambient partial pressure and isotopic values were obtained following Soued and Prairie (2020)³⁹ and partial pressure (ppmv) was converted to concentration (μM) considering alkalinity, following Koschorreck *et al.* (2021)⁴⁰.

4.2 Diffusive fluxes

Diffusive flux of CH₄ and CO₂ at the air - water interface was measured by means of an opaque floating chamber following Baliña *et al.* (2022b)³⁶, Suppl. Inf. 4). The diffusive flux rates (f_{gas}) were calculated in mmol

m² d⁻¹, following equation S2. All chamber measurements were inspected for bubble events based on whether there was an abrupt increase of CH₄ or the pattern of CH₄ increase over time was not following a strong linear relationship. All chamber measurements were performed during the daytime.

4.3. Gas transfer velocity

Gas transfer velocities (*K*) were calculated based on floating chamber measurements of gas exchange carried out inside the mesocosms and in the lake³⁶ (Suppl. Inf. 5, equation S3). The obtained values of *K* were standardized to a Schmidt number of 600 (equation S4). Given that the mesocosms were well mixed (Fig. S3 and S4), *K*₆₀₀ (m h⁻¹) can be expressed as an evasion decay constant (*K*_{EVA}, h⁻¹) when divided by the depth of the mesocosm (0.8 m) and was used for the mesocosm CH₄ mass balance calculations (see section 6).

5. Methane Oxidation (MOX) rates

To estimate CH₄ oxidation (MOX) rates, dark incubations were carried out for each lake (scheme of the workflow and specific details in Fig. S5). Since MOX follows first order kinetics, the instantaneous CH₄ oxidation rate (h⁻¹) for each lake or mesocosm can be obtained as the slope of the regression between ln (dissolved CH₄) (μM) vs Time (h)³². This estimate of oxidation decay constant (*K*_{MOX}) was used for the mesocosm CH₄ mass balances calculations (see section 6 below).

6. Mesocosm mass balances

Given that the mesocosms were closed at the bottom and impermeable to gases, and since the mesocosms remained fully oxic during the entire length of the experiment (Fig. S4), any observed inputs of CH₄ would have to originate from the mesocosm itself, and this would correspond to OMP. Therefore, the change in CH₄ concentration between two consecutive time points would be the result of the CH₄ produced, minus the CH₄ oxidized and diffused to the atmosphere (equation 1):

$$\Delta CH_4 = OMP - (EVA + MOX) \quad \text{eq. 1}$$

Where, ΔCH_4 is the change in CH₄ concentration between two consecutive time points, *OMP* stands for oxic methane production rate, *EVA* reflects the rate of CH₄ evasion to the atmosphere through diffusion, and *MOX* is the rate of CH₄ oxidation. If there was no production of CH₄ inside the mesocosms (*OMP* = 0), the concentration of CH₄ inside the enclosures would continuously decline to eventually equilibrate with the atmosphere, at a time frame that is dependent on the initial CH₄ concentration and the total CH₄ loss rate (*EVA* + *MOX*). Following this reasoning, CH₄ concentrations above what would be expected based on the total CH₄ loss would necessarily be due to OMP inputs.

The OMP component from equation 1 cannot be directly measured, but it can be indirectly derived from the rest of the components of the mass balance: CH₄ concentration was measured in the mesocosms at each time point; the evasion rate was measured with floating chambers (Section 4); and the MOX rate was

estimated through dark incubations (Section 5). The CH₄ data obtained at each time point allows us to build an empirical curve describing the behavior of CH₄ through time. This observed curve can be further compared to theoretical curves that predict the expected CH₄ concentration in the mesocosm at each time point if only processes of loss due to oxidation (equation 2), evasion (equation 3) or both (equation 4), were occurring. These theoretical curves were calculated based on the K_{eva} from the diffusive flux data (Section 4.3), and the K_{oxi} estimated from experimentally derived MOX data (Section 5). If the observed curve is higher than the theoretical curve modeled based on CH₄ loss both from oxidation and evasion (equation 4), this implies an excess of CH₄ relative to the expected concentration, indicating input from OMP.

$$[CH_4]_t = [CH_4]_{t0} * \exp(-K_{MOX} * t) \quad \text{eq. 1}$$

$$[CH_4]_t = [CH_4]_{t0} * \exp(-K_{EVA} * t) \quad \text{eq. 2}$$

$$[CH_4]_t = [CH_4]_{t0} * \exp(-K_{(MOX+EVA)} * t) \quad \text{eq. 3}$$

Where [CH₄]_t corresponds to the modeled concentration of CH₄ at a given time point (t, in μM), [CH₄]_{t0} corresponds to the concentration of CH₄ at time zero of the mesocosm experiment (t₀, μM), K_{MOX} corresponds to the decay constant of MOX (h⁻¹), t corresponds to a given time (h) and K_{EVA} corresponds to the decay constant of evasion (h⁻¹).

To solve the mass balance proposed in eq. 1 we used an approach based on estimating the change in the mass of CH₄ between consecutive time points, by multiplying the slope of the CH₄ concentration vs time for each segment by the respective delta time (Fig. 1C), both for the ambient concentrations (Fig. 1C panel A), and the modeled concentrations based on equation 4, for each mesocosm for the entire length of the experiment (Fig. 1C, panel B). We should point out that CH₄ concentrations declined in all mesocosms through time, so the approach described above involved reconstructing the patterns of loss in observed and predicted CH₄ concentrations, and comparing the resulting remaining masses of CH₄ to derive potential OMP rates in each mesocosm. Positive differences between these remaining masses represent the mass of CH₄ produced through OMP, and all the mesocosms yielded positive estimates.

Although the water used for the mesocosms was degassed through a shower head device during filling, the initial mesocosm CH₄ concentrations differed greatly (by orders of magnitude) between mesocosms of the different lakes, reflecting the vastly different ambient lake concentrations at the time. Given that we are modeling CH₄ losses as first order processes, which depend on initial CH₄ concentrations, we standardized the observed and modeled CH₄ concentrations in each mesocosm to their respective initial concentration to remove potential biases induced by large differences in initial ambient concentrations and thus render comparable OMP rates. Using these standardized concentrations (unitless), we derived OMP rates following the scheme presented in Fig. 1C, which yielded OMP rates in units of time⁻¹ rather than as μM time⁻¹. In Fig. S6 we present the observed concentrations as a function of time for each mesocosm that are the basis for these calculations.

The uncertainty around the modeled curves (MOX, EVA, and MOX + EVA) was estimated using Monte Carlo simulations. These simulations incorporated the variability in the model parameters, which were the mean and standard deviation of K_{MOX} and K_{EVA} specific to each lake, and the mean and standard deviation of the standardized initial CH_4 concentration for each mesocosm. For each simulation, random parameter values were sampled from normal distribution curves defined by these means and standard deviations, and the model was repeatedly evaluated over the range of time points. The resulting ensemble of model outputs was then used to calculate the mean predicted curve and its associated uncertainty.

7. OMP contribution to total lake CH_4 diffusive flux (OMC)

To estimate the contribution of OMP to total lake CH_4 emissions, we compared the standardized OMP rates (day^{-1}) determined in the mesocosms to the standardized CH_4 diffusive fluxes from the lakes (day^{-1}) (equation 7). CH_4 diffusive fluxes from the lakes were standardized to the CH_4 concentration in the lake at the moment of the diffusive flux measurement, and also to the area and volume of the lake. The surface area of the lake is known from studies done previously in the area³⁶ and the volume was obtained as the mean depth (m) multiplied by the surface area (m^2).

$$OMC (\%) = \frac{(standardized\ OMP * 100)}{standardized\ lake\ Flux} \quad eq.7$$

Where *OMC* is the contribution of OMP to lake CH_4 emissions (%), *standardized OMP* is the standardized aerobic CH_4 production measured in the mesocosms (d^{-1}) and *standardized lake Flux* is the standardized CH_4 diffusive flux measured in the respective lake (d^{-1}). OMC was calculated for each measured CH_4 diffusive flux in each lake.

8. Mesocosm isotopic mass balances

To calculate ^{13}C values of CH_4 potentially associated with oxic production, ($\delta^{13}C-CH_4-OMP$), a two-step isotopic mass balance was carried out. First, the measured $^{13}C-CH_4$ in the mesocosmos was corrected to remove the effect of fractionation due to evasion and oxidation. The fractionation factor of evasion (α_{eva}), a value of 1.0008, was obtained from the literature⁴¹. The fractionation factor of oxidation (α_{ox}) was calculated using data from our own dark incubations. The slope from the regression between $\ln [CH_4]$ vs $\ln (^{13}C-CH_4 + 1000)$ was used to obtain α_{ox} using equation 8.

$$\alpha_{ox} = \frac{slope}{1 + slope} \quad eq.8$$

Subsequently, $^{13}C-CH_4$ was corrected for evasion and oxidation using equation 9.

$$\delta^{13}CH_4_{corr} = \frac{Evasion}{Evasion+MOX} * (\delta^{13}CH_4_{ambient} - (\alpha_{eva})) + \frac{MOX}{Evasion+MOX} * (\delta^{13}CH_4_{ambient} - (\alpha_{mox})) \quad eq. 9$$

Where $\delta^{13}CH_4_{corr}$ corresponds to the $^{13}C-CH_4$ corrected by evasion and oxidation, *Evasion* corresponds to the expected rate of EVA ($\mu M\ hr^{-1}$) for each enclosure and each time point, which was obtained from the modeled curve considering only loss of CH_4 through evasion. *MOX* correspond to the expected rate of MOX

($\mu\text{M hr}^{-1}$) for each enclosure and time point, which was obtained from the modeled curve considering only loss of CH_4 through oxidation. $\delta^{13}\text{CH}_4^{\text{ambient}}$ corresponds to the $^{13}\text{C}-\text{CH}_4$ of measured CH_4 in the water column of the mesocosm, α_{eva} and α_{mox} are the fractionation factors, both in delta form (‰), obtained as $((\alpha - 1) * 1000)^{32}$.

$\delta^{13}\text{CH}_{4\text{corr}}$ was further used along with the $^{13}\text{C}-\text{CH}_4$ of the water used to fill the mesocosms at the onset of the experiment to derive the $\delta^{13}\text{C}-\text{CH}_{4\text{-OMP}}$ following equation 10.

$$\delta^{13}\text{CH}_{4\text{OMP}} = \frac{(CH_{4\text{zero}} * \delta^{13}\text{CH}_{4\text{zero}}) + (CH_{4Tx} * \delta^{13}\text{CH}_{4\text{corrTx}})}{(CH_{4\text{zero}} + CH_{4Tx})} \quad \text{eq. 10}$$

Where $\delta^{13}\text{CH}_{4\text{OMP}}$ is the ^{13}C of CH_4 produced through OMP, $CH_{4\text{zero}}$ and $\delta\text{CH}_{4\text{zero}}$ are the concentration (μM) and the $^{13}\text{C}-\text{CH}_4$ of the water used to fill the mesocosm, respectively; CH_{4Tx} is the concentration of CH_4 (μM) at any given time point and $\delta^{13}\text{CH}_{4\text{corrTx}}$ is the $^{13}\text{C}-\text{CH}_4$ at that given time point, which was previously corrected for fractionation due to evasion and oxidation. We estimated $\delta\text{CH}_{4\text{OMP}}$ for each time point of the experimental mesocosm time course, and here we report the average value for the entire experiment.

9. Phytoplankton cultures

To assess the potential for CH_4 production by phytoplankton present in the study lakes, phytoplankton species were isolated from each one of the three lakes. Water from SA, SG and BU was collected and filtered through a $55\text{ }\mu\text{m}$ net to exclude macro and mesozooplankton, on the 5th of May 2022. The water was transported to the laboratory, where it was inoculated in petri dishes with agar mediums BG11⁴², Bold's Basal Medium⁴³ (BBM), BBM + Vitamins (cyanocobalamin, thiamine and biotin) and BBM + soil extract (3:1, v/v), in all cases using the spray technique⁴⁴. Three petri dishes per medium and lake were inoculated, obtaining a total of 48 inoculated plates. These were kept under controlled conditions of light (photoperiod 12:12 light: darkness) and temperature (25°C). Weekly identification of growing colonies was done using a magnifying scope (Nikon SMZ 745T). When a colony was detected, it was removed from the petri dish under sterile conditions, observed in an Olympus BX50 optical microscope to identify the genera using specific bibliography^{45–47} and afterwards it was inoculated in another petri dish with the same growth medium for further isolation. Further experiments were carried out with 4 genera of chlorophytes and 3 genera of cyanobacteria that were particularly prevalent in the lakes.

10. Experiments to measure methane production by algal strains using membrane inlet mass spectrometry (MIMS)

Experiments were carried out to assess the potential production of CH_4 by the phytoplankton isolates using a membrane inlet mass spectrometer (MIMS, Bay-Instruments, Fig. S7)²⁴. Each culture was placed in a 3.5-ml glass chamber that was surrounded by an acrylic jacket connected to a recirculating water bath used to maintain the culture at a constant temperature of 25°C . The culture chamber was located above a stirrer, to ensure mixing and to avoid gradients, and it was exposed to a photoperiod of 15 h light: 9 h darkness,

at a light intensity of $120 \mu\text{mol photons m}^{-2} \text{ s}^{-1}$. The culture chamber had an inlet and an outlet and the culture fluid was continually circulated through the MIMS exchanger by means of a small peristaltic pump. O_2 and CH_4 in the culture were measured every 12 seconds, and only one culture at a time could be processed. The extent of MIMS physical loss depends on CH_4 concentration within each culture: to characterize this physical CH_4 loss, autoclaved cultures were employed to establish a connection between the initial CH_4 concentration in a culture and the rate of physical CH_4 loss through the MIMS. Since these were dead cultures, they lack biological fluctuations in CH_4 concentration and solely exhibit CH_4 loss due to physical factors. Leveraging this dataset, a linear relationship between the initial CH_4 concentration and the rate of physical loss was derived. This correlation was subsequently used to estimate the physical loss for each measured culture, considering their initial CH_4 concentration (Fig. S8). Each experiment lasted between three to five days, and two to three experiments were carried out for each culture. As negative controls, ultrapure water and sterile BG11 culture media were used.

At the beginning and end of each experiment, chlorophyll a (Chla) was measured and ambient DNA was extracted from the culture (Suppl. Inf. 6). Chla measurements were done to standardize phytoplankton-derived methane production rates to biomass, whereas DNA extraction followed by PCR was carried out to test for the presence of methanogenic archaea and methanotrophic bacteria.

10.1. Phytoplankton methane production rates

Phytoplankton methane production rates were calculated using the Stavisky-Golay function from the Signal package in R (<http://r-forge.r-project.org/projects/signal/>)²⁴. First, CH_4 concentration vs time interval curves were smoothed using the `sgolay` function, fitting a polynomial of second degree and no derivative. The `sgolay` function was then used to obtain the first derivative of this smoothed curve - which corresponds to the rate - also fitting a second-degree polynomial. The rate thus obtained was then corrected for the rate of physical loss of gas from the experimental setup (derived as described above) and was standardized to the Chla concentration of each culture.

Results

1. Limnological characteristics

Mesocosms of SG had a higher transparency, lower total phosphorus (TP), total nitrogen (TN), total suspended solids (TSS) and phytoplankton abundance than the mesocosms of SA and BU (Table 1). Compared to SA, the mesocosms in BU had higher levels of turbidity and TSS and subsequently, a higher K_{dpar} and lower euphotic depth. The mesocosms in SA had a higher Chla than the mesocosms of BU. The BU mesocosms were dominated by smaller phytoplankton species that occurred at a higher abundance, whereas the SA mesocosms had the opposite pattern, with larger phytoplankton species dominating. Concentrations of dissolved organic carbon (DOC), dissolved inorganic carbon (DIC), dissolved O_2 , and O_2 saturation levels were generally high and comparable across the mesocosms of all three lakes. Based on the diel variability on O_2 , the mesocosms from SG were on average net heterotrophic, whereas the

mesocosms from SA and BU were on average net autotrophic. All the studied lakes were on average net autotrophic.

Table 1. Mean \pm standard values for mesocosms (M) and the lake (L).

Parameters	SG		SA		BU	
Treatment	M	L	M	L	M	L
$K_{dpar} (m^{-1})$	1.86 ± 0.42		4.37 ± 0.08		8.53 ± 1.93	
Secchi depth (m)	NA		0.38 ± 0.05		0.19 ± 0.01	
Euphotic depth (m)	2.6 ± 0.6		1.03 ± 0.05		0.56 ± 0.11	
Water T ($^{\circ}C$)	23.02 ± 3.17	22.86 ± 3.23	27.78 ± 2.22	27.85 ± 2.12	23.08 ± 1.70	22.71 ± 1.71
pH	9.3 ± 0.17	9.41 ± 0.07	9.46 ± 0.02	9.41 ± 0.04	9.15 ± 0.03	9.06 ± 0.06
Dissolved CH_4 ($\mu mol L^{-1}$)	26.02 ± 24.45	33.37 ± 39.20	0.42 ± 0.21	1.48 ± 0.28	0.04 ± 0.04	0.27 ± 0.03
Dissolved O_2 ($mg L^{-1}$)	7.73 ± 0.49	10.86 ± 5.13	10.01 ± 1.68	10.21 ± 2.72	10.99 ± 0.96	11.13 ± 1.13
O_2 saturation (%)	90.18 ± 10.23	128.79 ± 67.43	128.37 ± 27.14	131.68 ± 41.13	127.79 ± 13.39	128.69 ± 16.72
Turbidity (NTU)	2.48 ± 0.78	2.10 ± 0.33	46.45 ± 10.27	46.15 ± 7.55	94.53 ± 8.84	107.25 ± 12.75
TSS ($mg L^{-1}$)	2.31 ± 0.56	3.60 ± 0.73	$24.35 \pm .46$	22.85 ± 3.35	55.50 ± 2.96	53.79 ± 0.21
DOC ($mg L^{-1}$)	38.86 ± 0.51	38.01 ± 1.28	44.12 ± 0.08	43.12 ± 0.39	36.59 ± 0.55	36.14 ± 0.36
DIC ($mg L^{-1}$)	98.58 ± 3.64	96.79 ± 3.44	108.65 ± 4.23	108.88 ± 0.67	81.21 ± 3.97	83.69 ± 0.08
TP ($\mu g L^{-1}$)	82.50 ± 19.38	75.00 ± 9.00	180.00 ± 44.90	183 ± 39	259.50 ± 33.91	288 ± 0.00
TN ($\mu g L^{-1}$)	2175 ± 417	2370 ± 330	2310 ± 475	1920 ± 0	2400 ± 983	2850 ± 570
Chla ($\mu g L^{-1}$)	2.45 ± 0.93	6.58 ± 1.41	117.14 ± 22.72	126.12 ± 0.71	87.09 ± 17.55	127.46 ± 4.74
Phytoplankton (ind mL^{-1})	1364.75 ± 463.05	2572.50 ± 399.50	113906.25 ± 18905.78	73287.50 ± 4104.50	148524.43 ± 32870.87	78454.00 ± 15270.00
Cyanobacteria (%)	24.56 ± 13.66	23.83 ± 5.24	1.05 ± 1.06	1.50 ± 0.70	72.14 ± 6.80	62.49 ± 4.32
Chlorophyta (%)	46.65 ± 12.21	31.79 ± 5.19	96.59 ± 1.05	95.44 ± 1.87	25.22 ± 5.33	33.67 ± 6.36
GPP ($g O_2 m^{-2} d^{-1}$)	0.47 ± 0.05	13.37 ± 0.33	6.24 ± 0.43	11.60 ± 0.68	4.91 ± 0.09	7.48 ± 0.09
RE ($g O_2 m^{-2} d^{-1}$)	0.59 ± 0.05	11.92 ± 0.41	6.98 ± 0.41	7.59 ± 0.64	4.60 ± 0.10	4.04 ± 0.10
NEP ($g O_2 m^{-2} d^{-1}$)	-0.21 ± 0.20	2.63 ± 4.50	0.99 ± 1.37	4.01 ± 0.41	1.97 ± 1.12	3.44 ± 1.15

The water temperature, (water T), pH, and O_2 concentration and saturation were measured at each time point. Turbidity, TSS, K_{dpar} , euphotic depth, DOC, DIC, TP, TN, Chla, phytoplankton abundance and composition were assessed at the beginning and end of each experiment. Dissolved CH_4 corresponds to the mean of all measurements throughout the experiment. T of the water, dissolved O_2 and O_2 saturation correspond to sub superficial values. NA means there is no data. Secchi depth was not registered in the lake SG because the submerged macrophytes do not allow a comparable measurement. For the lake, GPP (gross primary production), ER (ecosystem respiration) and NEP (net ecosystem production) correspond

to the daily mean for the one miniDOT, whereas for the mesocosms the values represent the daily mean of the miniDOTs deployed in the replicate mesocosms.

Phytoplankton community composition differed between the three lakes but was similar between the lake and the corresponding mesocosms (Fig. S9). In SG the dominant genera were *Chlamydomonas* sp. and *Didymocystis* sp. (Chlorophyta), *Cryptomonas* sp. (Cryptophyta) and *Coelosphaerium* sp. (Cyanobacteria). In SA, there was an almost complete dominance of *Scenedesmus linearis* (Chlorophyta) (52% - 68% of the total phytoplankton abundance) followed by *Oocystis* sp., *Eutetramorus* sp. and *Cosmarium* sp. (Chlorophyta). In BU, the dominant genera were *Monoraphidium* sp, *Oocystis* sp., and *Scenedesmus* sp. (Chlorophyta), and *Planktolyngbya* sp., *Geitlerinema* sp. and *Anabaenopsis* sp. (Cyanobacteria).

Methanogenic archaea were detected in water samples of all three lakes and their respective mesocosms (Fig. S10a). The class Methanomicrobia was the most widespread methanogenic group and was detected in all three lakes and their mesocosms, whereas the class Methanobacteria was only detected in the lake and mesocosms of SG. Methanotrophic bacteria were also detected in water samples of all three lakes and their respective mesocosms (Fig. S10b). Methanotrophs from the class gammaproteobacteria were detected and most abundant in all lakes and mesocosms, whereas metanotrophs from the class alphaproteobacteria was detected in mesocosms and lake in BU and SA, but in SG only in the mesocosms at the end of the experiment.

2. CH₄ dynamics in lakes and experimental mesocosms

2.1. Patterns in dissolved CH₄ and $\delta^{13}\text{C}$ -CH₄

The lakes differed greatly in ambient surface water CH₄ concentration at the time of mesocosms deployment, with average concentrations of $122.8 \pm 10.9 \mu\text{M}$, $1.5 \pm 0.2 \mu\text{M}$ and $0.3 \pm 0.1 \mu\text{M}$ for SG, SA and BU, respectively (Fig. S11 a, c and e). CH₄ concentrations in the mesocosms were consistently lower than in the surrounding lake, suggesting partial degassing during filling. The initial CH₄ concentration in the mesocosms at the onset of the experiments nevertheless differed by orders of magnitude between lakes, still reflecting ambient lake differences: $65.1 \pm 5.7 \mu\text{M}$, $0.9 \pm 0.1 \mu\text{M}$ and $0.1 \pm 0.0 \mu\text{M}$ for SG, SA and BU, respectively (Fig. S11 b, d and f). CH₄ concentrations subsequently declined in all mesocosms during the experimental time course, whereas in lakes the dynamics of surface water CH₄ followed different patterns (Fig. S9 a - f). The isotopic composition of ambient CH₄ (^{13}C -CH₄) generally ranged between -20 ‰ and -40 ‰ in both the lake and the mesocosms (Fig. S11 g - i), except for a period of very depleted CH₄ that occurred in BU mesocosms between 45h and 75h (up to -60 ‰).

2.2 CH₄ exchange velocity and diffusive fluxes

Diffusive CH₄ fluxes were higher in the lakes than in the mesocosms (Fig. S12a), which is expected given that the lakes had both higher ambient CH₄ concentrations and higher exchange velocities (Fig. S12b). The mean CH₄ diffusive fluxes from the lakes were $24.7 \pm 13.5 \text{ mmol m}^{-2} \text{ d}^{-1}$, $21.6 \pm 19.5 \text{ mmol m}^{-2} \text{ d}^{-1}$, and $0.5 \pm 0.1 \text{ mmol m}^{-2} \text{ d}^{-1}$ for SG, SA and BU, respectively, whereas the mean fluxes in the mesocosms were 0.6

± 0.4 mmol m⁻² d⁻¹, 0.2 ± 0.1 mmol m⁻² d⁻¹ and 0.02 ± 0.00 mmol m⁻² d⁻¹ for SG, SA and BU, respectively. Similarly, gas exchange velocities were consistently higher in the lakes than in the mesocosms (Fig. S12b), likely because mesocosms are sheltered from the wind due to the protective rim on the side and reduced overall turbulence. The mean K₆₀₀ CH₄ for the lake were 0.7 ± 0.1 m d⁻¹, 2.0 ± 0.2 m d⁻¹, and 1.6 ± 0.5 m d⁻¹ for SG, SA and BU, respectively, whereas the mean K₆₀₀ CH₄ for the mesocosms were 0.1 ± 0.0 m d⁻¹, 1.2 ± 0.4 m d⁻¹ and 0.6 ± NA m d⁻¹ for SG, SA and BU, respectively. The estimated K_{eva} were 0.01 h⁻¹, 0.06 h⁻¹ and 0.03 h⁻¹ for SG, SA and BU, respectively.

3. Methane oxidation (MOX) rates

We observed a consistent decrease in CH₄ concentrations and a concomitant enrichment of δ¹³C-CH₄ in all dark in vitro incubations, suggestive of CH₄ oxidation (Fig. S13). The estimated CH₄ oxidation decay constants (K_{oxi}) averaged 0.03 h⁻¹, 0.01 h⁻¹ and 0.02 h⁻¹, for SG, SA and BU, respectively (Fig. S14).

4. Estimates of OMP rates and isotopic signature of CH₄ derived from oxic production (δ¹³C-CH₄-OMP)

4.1 OMP rates and OMC

At almost every time point in all mesocosms (except 21h) the observed CH₄ concentration exceeded the modeled CH₄ concentration based on the combination of MOX + EVA, suggesting CH₄ production in all the mesocosms throughout the experiments (Fig. 2). A plot indicating MOX and EVA curves separately can be found in Fig. S15. The estimated (standardized) OMP rates in the mesocosms of each lake, derived as described in section 6 of methods, were 0.01 ± 0.00 day⁻¹, 0.07 ± 0.01 day⁻¹, and 0.07 ± 0.01 day⁻¹ for SG, SA and BU, respectively (Table 2).

The contribution of OMP to total lake CH₄ diffusive flux (OMC) ranged between 0.3 and 6.7 % depending on the lake (Table 2).

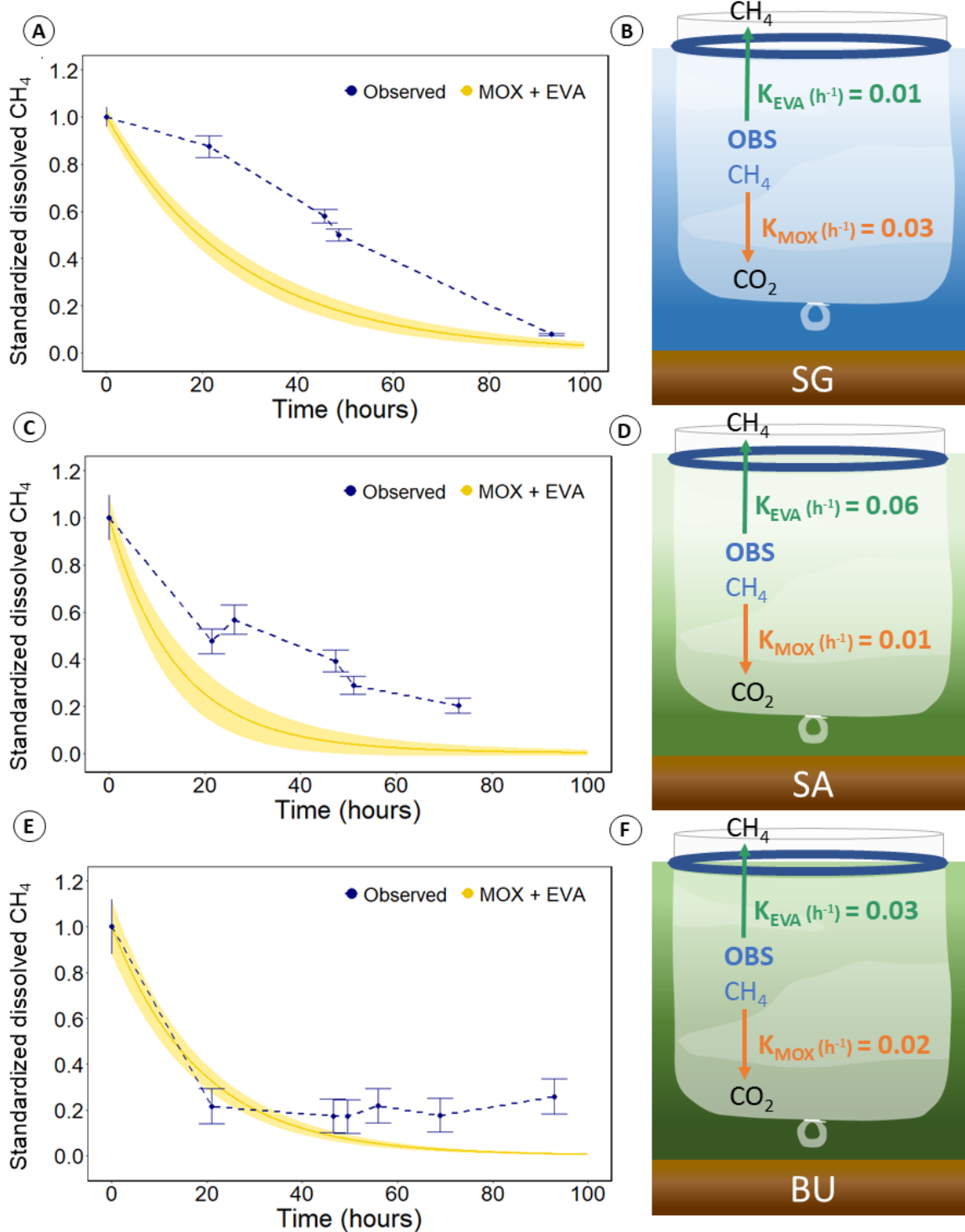
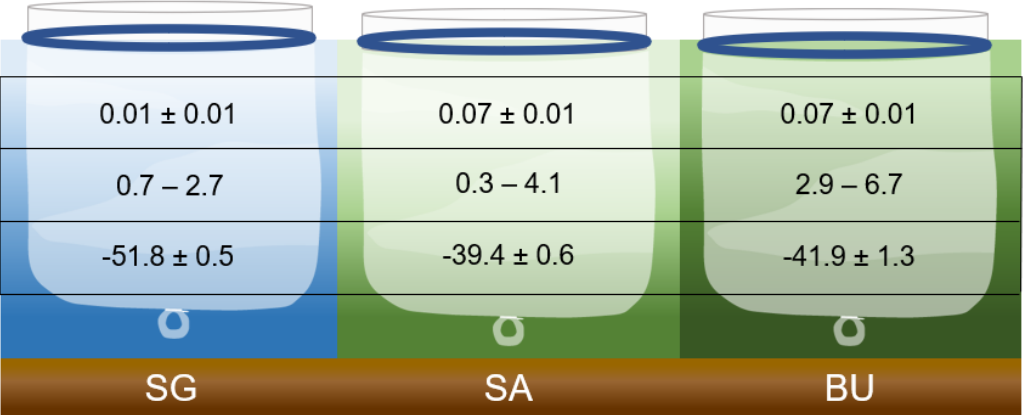


Figure 2. Observed (blue) and theoretical curves indicating CH_4 loss in the mesocosm only by oxidation (orange), by evasion (green) or by both processes (yellow) for SG (a), SA (c) and BU (e). Decay constant of evasion (K_{EVA}) and oxidation (K_{MOX}) for each lake system, SG (b), SA (d) and BU (f).

4.2 Isotopic signature of CH_4 derived from oxic production ($\delta^{13}\text{C}-\text{CH}_4\text{-OMP}$)

We used an isotopic mass balance approach to derive the potential isotopic signature of CH₄ produced under oxic conditions in the mesocosms. For this mass balance, fractionation factors for CH₄ oxidation (α_{oxi}) were derived from the in vitro MOX dark incubations, and were estimated at 1.02, 1.03 and 1.21 for SA, SG and BU, respectively (Fig. S16). α_{oxi} for BU was too high and the R² of this regression (0.83) was weaker than that of the regression for SA (0.99) and SG (0.99). This was presumably related to the fact that in BU CH₄ concentration was very low, which made it difficult to measure ¹³C-CH₄ precisely. Accordingly, we assumed that the α_{oxi} of BU = SA, since both were turbid phytoplankton-dominated lakes. The estimated ¹³C-CH₄ OMP for the mesocosms was consistently enriched relative to the isotopic values of CH₄ produced in the surrounding sediments (-62.21 ± 0.14 to -59.81 ± 1.11, unpublished data from these lakes). $\delta^{13}\text{C-CH}_4\text{-OMP}$ for SA and BU were similar, whereas SG had even more enriched values (Table 2).

Table 2. Standardized OMP rates (day⁻¹), contribution of OMP to total lake CH₄ emissions (OMC, %) and ¹³C-CH₄ OMP for the three studied lakes.



Std OMP (day ⁻¹)	0.01 ± 0.01	0.07 ± 0.01	0.07 ± 0.01
OMC (%)	0.7 – 2.7	0.3 – 4.1	2.9 – 6.7
$\delta^{13}\text{C-CH}_4\text{OMP}$ (‰)	-51.8 ± 0.5	-39.4 ± 0.6	-41.9 ± 1.3
	SG	SA	BU

5. In vitro experiments to assess phytoplankton CH₄ production

Four Chlorophyte (*Scenedesmus linearis*, *Scenedesmus quadricauda*, *Monoraphidium circinale*, *Oocystis lacustris*) and three Cyanobacteria (*Phormidium* sp., *Leptolyngbya* sp., *Pseudanabaena* sp.) strains isolated from the three studied lakes were probed for potential CH₄ production with a protocol using MIMS. As controls, Mili-Q water (Fig. S17a) and BG11 medium (Fig. S17b) were used, all of them being equilibrated with sterile-filtered air before measurement in the MIMS. Milli-Q water did not show any changes in CH₄ concentration through time, as expected. Likely because the BG11 medium was not sufficiently equilibrated, there was a slight decrease in CH₄ and O₂ concentrations through time. All tested cultures were alive and had a clear and recurrent diurnal pattern of photosynthesis and respiration as reflected in variations in O₂ concentrations. The results from two cultures, *Leptolyngbya* sp. and *Oocystis* sp. are shown as examples (Fig. 3). All tested cultures showed increases in CH₄ concentration during light hours, followed by decreases during the dark, and there was a strong overall coherence between the diurnal patterns in O₂ and those of CH₄ (Fig. 6a). No methanogenic archaea nor methanotrophic bacteria were detected in any of the phytoplankton cultures (Fig. S18). This implies that the observed increases of CH₄ in

light conditions can only be attributed to phytoplankton and related to photosynthesis, since there are no other methanogenic organisms present in the culture. On the other hand, the decrease in CH₄ during dark hours must be related to the physical CH₄ loss from the system that offset the decrease in CH₄ production in the dark, since there was no apparent biological CH₄ consumption in the cultures. From the diurnal variations in CH₄ concentrations we were able to derive CH₄ production rates for each of the cultures over several diurnal cycles, and table 3 shows the mean CH₄ production rate for each culture for the ensemble of incubations that were carried out for each culture. These rates represent the mean CH₄ production per g of Chla and per hour of a 24-hour cycle. CH₄ production rates ranged between 0.02 to 0.20 $\mu\text{mol CH}_4 \text{ g Chla}^{-1} \text{ h}^{-1}$, and no significant differences between Chlorophyta and Cyanobacteria were detected, although within each group there were taxa that had significantly higher production rates.

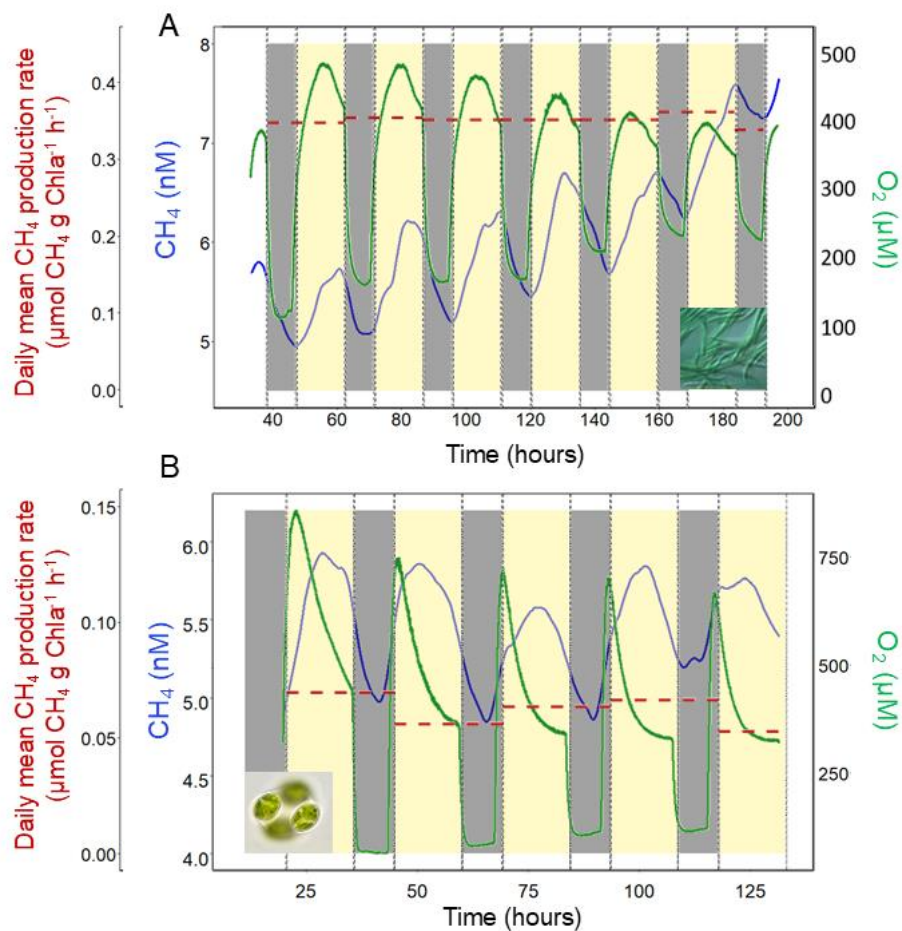


Figure 3. Dissolved CH₄ and O₂ in the culture and derived phytoplankton CH₄ production daily mean rates, for one of the measurements of *Leptolyngbya* sp. (A) and of *Oocystis* sp. (B). Yellow columns correspond to hours of light and grey columns correspond to hours of dark. Picture of *Leptolyngbya* sp. taken from Culture Collection, picture from *Oocystis* sp. taken from AlgaeBase.

Table 3. Mean methanogenesis rates ($\mu\text{mol CH}_4 \text{ g Chla}^{-1} \text{ h}^{-1}$) for the phytoplankton isolates analyzed in the MIMS.

	Phytoplankton strain (genera or specie)	Mean CH_4 production rate ($\mu\text{mol CH}_4 \text{ g Chla}^{-1} \text{ h}^{-1}$)	Standard deviation CH_4 production rate ($\mu\text{mol CH}_4 \text{ g Chla}^{-1} \text{ h}^{-1}$)
Chlorophyta	<i>Scenedesmus linearis</i>	0.07	0.04
	<i>Scenedesmus quadricauda</i>	0.09	0.01
	<i>Monoraphidium circinale</i>	0.04	0.00
	<i>Oocystis lacustris</i>	0.06	0.04
Cyanobacteria	<i>Leptolyngbya</i> sp.	0.20	0.15
	<i>Phormidium</i> sp.	0.02	0.01
	<i>Pseudoanabaena</i> sp.	0.09	0.02

Discussion

Although there is now widespread consensus on the existence of CH_4 production within the oxic water column of lakes^{6,33,48}, there is still uncertainty as to the actual mechanisms involved, their dynamics, and the contribution of these pathways to the overall CH_4 production in various types of freshwater ecosystems^{31,49–51}. The contribution of OMP to total CH_4 emissions varies greatly among ecosystems but has been suggested to be a function of system morphometry, increasing with mean depth and the ratio of volume to sediment area^{31,32}. It would then be expected that the contribution of OMP should be lower in small and / or shallow lakes, where CH_4 inputs are dominated by sediment and littoral sources, yet there have been very few studies that have assessed the potential contribution of OMP in these systems²³. There is also indication that OMP may be linked to ambient algal biomass and primary production^{20,21}, and there is increasing evidence from in vitro studies that phytoplankton produce CH_4 . This is one of the pathways that has been invoked to explain OMP^{7,17,21}, although the contribution of algae to ambient OMP has yet to be defined. All phytoplankton taxa tested to date produce CH_4 in culture, albeit at very different rates depending on algal biomass, primary production, temperature and light exposure, among others^{22,24,25,27}, suggesting that community composition and environmental conditions both play a role in shaping the observed patterns of OMP. In this regard, many shallow lakes in the world are very productive and develop high phytoplankton biomass, and it would be expected that the contribution of OMP could potentially be high in these lakes despite their morphometry, but this hypothesis has seldom been tested. In addition, the phytoplankton communities of shallow lakes may be dominated by entirely different taxa⁵², and these contrasts in community composition could potentially lead to differences in ambient OMP as well. To test these contrasting hypotheses, we quantified the magnitude and contribution of OMP in shallow lakes of the Pampean Plain that differed greatly in both the abundance and composition of their phytoplankton

communities. We further assessed the potential for the dominant phytoplankton taxa to produce CH₄ and evaluated the contribution of phytoplankton to the observed OMP in these lakes.

We detected OMP in all mesocosms, albeit at very different rates. Mean standardized OMP rates (SG 0.01 day⁻¹, SA 0.07 day⁻¹ and BU 0.07 day⁻¹) were obtained using standardized CH₄ concentrations, as explained in the methods section, in units of day⁻¹. The isotopic mass balances revealed an isotopic signature for the CH₄ produced through OMP that was much more enriched than the CH₄ produced in the sediment, and more similar to the one of oxidized CH₄. There are not many studies that have explored the potential isotopic signature of the CH₄ produced through OMP, but the few studies that have done so, have also reported enriched signatures for the OMP-CH₄. Using isotopic whole-lake mass balances, Thottathil *et al.* (2022)³² reported $\delta^{13}\text{C}$ -CH₄ OMP values for four Canadian lakes ($-38.0 \pm 1.4\text{‰}$ to $-63.6 \pm 2.2\text{‰}$) that were greatly enriched relative to anoxic sediment sources. In line with this, Klintzsch *et al.* (2023)²⁵ explored the isotopic values of CH₄ produced directly by different cultures of marine phytoplankton species, which ranged from $-19.3 \pm 0.9\text{‰}$ to $-54.5 \pm 1.6\text{‰}$, implying a uniquely enriched signature for phytoplankton-derived CH₄. Similarly, Taenzer *et al.* (2020)³⁵ carried out marine water incubations and reported a MPn-derived $\delta^{13}\text{C}$ -CH₄ of $-40 \pm 5\text{‰}$, indicating also an enriched $\delta^{13}\text{C}$ -CH₄ for MPn derived CH₄. These results have implications, because they imply that the isotopic signature of CH₄ in the water column does not just account for oxidation, but potentially also for the confounding influence of CH₄ production within the water column.

Estimating OMP rates at an ecosystem scale is extremely challenging, because it involves the quantification of many different processes with high spatio-temporal dynamics, that cannot be directly measured and therefore must be derived from other measurable processes, usually through a mass balance. The mesocosm experiments allowed us to constrain the mass balance components by excluding sediment CH₄ production, CH₄ bubble dissolution and lateral transport. However, CH₄ oxidation and CH₄ diffusive flux to the atmosphere remained a challenge. We estimated MOX using dark incubations, as was done by Bogard *et al.* (2014)²⁰ and Thottathil *et al.* (2022)³². We are aware, however, that MOX rates are affected by CH₄ concentration, O₂ concentration and potentially by light irradiance, where the latter seems to result in MOX inhibition^{53–55} (but also see^{56,57}). CH₄ and O₂ concentrations were roughly similar between the incubations and the mesocosms, but light irradiance was higher in the latter. Therefore, dark incubations could have led to an overestimation of MOX rates, which translates into an overestimation of OMP rates from the mass balance. Conversely, in MOX incubations potential OMP from methylated substrates was not excluded, which would result in an underestimation of MOX and therefore an underestimation of OMP rates from the mass balance. We are confident, however, that our oxidation data are sound overall, because they are based on robust oxidation curves (Figures S11 and S12) and coherent MOX rates that fall well within values reported for other lakes^{29,31,32}. Regarding CH₄ diffusive fluxes, repeated measurements were taken in all mesocosms and lakes. We acknowledge, however, that diffusive fluxes can vary significantly with weather conditions, and to minimize this variability, we carried out mass balances using average gas exchange velocities and wind speeds.

When compared to other standardized OMP rates reported in the literature, which for the most part had much lower chlorophyll concentrations, our lakes were on the lower end (Fig. S19b). Despite being eutrophic to hypertrophic, these shallow lakes had OMP rates that were either within the range, or lower than what has been reported for lakes with much lower chlorophyll concentrations (Fig. S19b). Previous studies had shown a relationship between chlorophyll concentration and OMP rates across a relatively narrow range of oligotrophic to mesotrophic temperate lakes^{20,32}, but these shallow, highly productive Pampean lakes do not fit this pattern at all. This suggests that chlorophyll is not a universal scaling variable for OMP across lakes, and that factors other than the absolute algal biomass present may drive OMP in lakes of different types^{7,23,29,30,48}.

In this regard, our own experimental results confirmed the production of CH₄ by phytoplankton strains that were dominant in these shallow lakes. In all cases, CH₄ production appeared to be linked to photosynthesis based on the coherence in the diurnal patterns of O₂ and CH₄. We observed CH₄ production from both Cyanobacteria and Chlorophyta genera, with CH₄ production rates ranging between 0.02 and 0.2 $\mu\text{mol CH}_4 \text{ g Chla}^{-1} \text{ h}^{-1}$. Our results add to the increasing body of evidence of widespread CH₄ production across major marine and freshwater phytoplankton groups^{21,24–27}. Our measured phytoplankton production rates were higher than those reported by Gunthel *et al.* 2020²¹ for a range of freshwater diatom strains ($\sim 0.004 \mu\text{mol CH}_4 \text{ g Chla}^{-1} \text{ h}^{-1}$), but similar to those reported by Bižić *et al.* (2020)²⁴ for cyanobacterial strains ($\sim 0.012 \mu\text{mol CH}_4 \text{ g Chla}^{-1} \text{ h}^{-1}$) (assuming a ratio of 1:50 of Chla to particulate organic carbon). We observed one order of magnitude range in CH₄ production among the strains tested but this range was not linked to light or nutrient availability since experimental conditions were similar for all strains, and there was not a clear difference in CH₄ production rates between major phytoplankton groups. There are probably intrinsic differences in metabolic pathways and growth responses between strains that shape these patterns of phytoplankton CH₄ production that require further exploration. Regardless of the underlying mechanisms, these experimentally derived rates can be extrapolated to the mesocosm field conditions to derive a first order estimate of the potential contribution of phytoplankton to ambient OMP. Our results suggest that the production of CH₄ by phytoplankton likely has a small contribution (<14%) of the estimated ambient OMP in the mesocosms, and this despite the high algal biomass and chlorophyll concentration that characterizes some of these systems. Studies have reported a positive influence of light exposure and intensity on phytoplankton CH₄ production under controlled conditions^{21,24,28}. In this regard, the growth media and light conditions used in the CH₄ production essays do not necessarily mimic the ambient conditions that these phytoplankton strains experience in situ, yet there is no reason to think that these strains would express CH₄ production rates that would be orders of magnitude higher in situ than in culture. All the evidence points to the fact that whereas the major phytoplankton groups in these shallow lakes do produce CH₄, these phytoplankton-linked CH₄ production rates account for only a small proportion of the observed OMP. This may explain the observed uncoupling between the estimated OMP and the ambient chlorophyll in these systems (Fig. S19).

CH₄ production as a by-product of MPn degradation in the process of phosphorus acquisition by bacteria is a widely known source of oxic CH₄ production in P-stressed waters^{2,10}. In the presence of phosphate, however, MPn degradation activity of bacteria can be repressed¹². Shallow Pampean lakes have high concentrations of phosphorus and, therefore, degradation of MPn is not expected to be a substantial CH₄ source, although this pathway cannot be discarded. Grossart et al. (2011)⁴ also reported that methanogenic archaea could attach to phytoplankton, possibly living in micro-anoxic niches, and this implies that they could potentially produce CH₄ through anaerobic methanogenesis but in the water column. Analysis of DNA from the water revealed the presence of 16S rRNA gene sequences of methanogens in all the mesocosms from the three shallow lakes. While this is no measure of methanogenic activity, we cannot exclude that archaea may have contributed to methane production in the mesocosms. In this regard, studies have further suggested a link between OMP and ambient primary production^{20,31}, assumed to reflect direct photosynthesis-related algal CH₄ production, but which may reflect the enhancement of other OMP pathways, including algal-associated archaeal methanogenesis. If such a connection exists, our results suggest that it is not scalable across systems, since our mesocosms had comparable OMP to those reported in oligotrophic and mesotrophic sites yet had rates of primary production that were many folds higher than those systems. In addition, methane production through photooxidation of organic matter^{58,59} and through bacterial degradation of dissolved organic matter (DOC)¹⁰ have also been reported as explanations for OMP. The three shallow lakes from this study exhibited high concentrations of DOC and high light irradiance, suggesting that these two pathways could also contribute to the observed OMP rates.

Our results imply that OMP is not the dominant pathway to the overall CH₄ diffusive emissions measured in these lakes, despite being eutrophic and highly productive. Previous studies have suggested that lake morphometry plays a role in determining the contribution of OMP to total CH₄ production or emission, in particular, the ratio of sediment area (A_{sed}) to mixed layer volume (V)^{31,32}. The results from the shallow lakes of this study are in good agreement with the patterns found in lakes elsewhere, and extend the reported patterns to a much wider range of values of A_{sed}/V (Fig. 4). This pattern suggests that CH₄ dynamics in these shallow lakes are overwhelmingly dominated by the production of CH₄ in the sediments, and this regardless of trophic status, phytoplankton biomass and composition, and ecosystem metabolism. At the other extreme are lakes where the water column is largely uncoupled from sediments, and where OMP plays a major role in determining CH₄ emissions, even when OMP rates may be low.

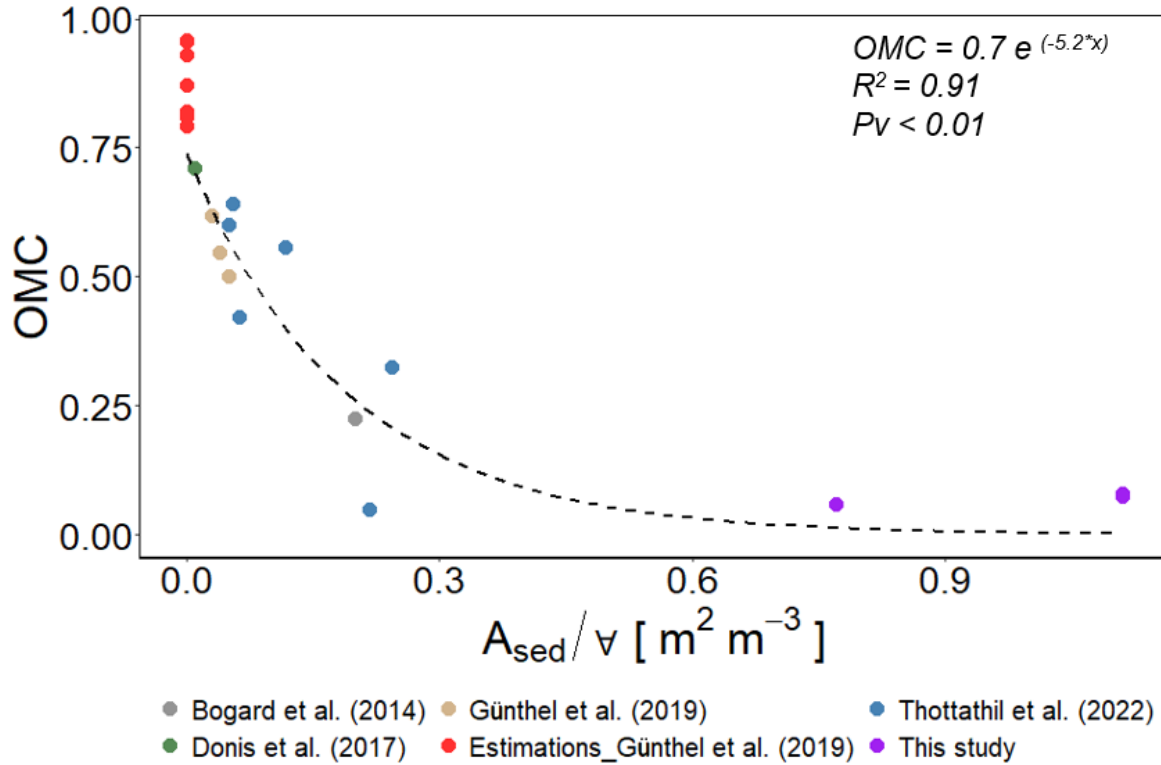


Figure 4. Relationship between oxie methane contribution (OMC) and lake morphometry, specifically, the ratio of sediment area (A_{sed}) to mixed later water column volume (V). For these shallow and polymictic lakes, the entire lake volume is considered as V . The colours represent different studies, and the data in purple dots correspond to this study.

In summary, by combining field mesocosm experiments with controlled laboratory experiments we were able to estimate ambient OMP rates and the contribution of this pathway to total CH_4 fluxes in three shallow lakes that differed in algal biomass and productivity. We were also able to infer the contribution of phytoplankton to estimated OMP rates (Fig. 5). We have shown that OMP rates in these eutrophic lakes were comparable to those reported in oligotrophic and mesotrophic lakes despite large differences in phytoplankton biomass and primary production. The contribution of OMP to CH_4 diffusive emissions (OMC) was modest (<14%), suggesting that in these shallow lakes, sediment processes overwhelmingly dominate CH_4 dynamics and OMP plays a minor role. Overall, the potential contribution of phytoplankton to OMP was low, even when assuming the maximum scenario obtained from the experimental results and despite the large algal biomass found in some of the lakes (Fig. 5). There was a slight increase in OMC, and in the contribution of phytoplankton to OMP with increasing phytoplankton biomass in these lakes, suggesting that OMP is not completely decoupled from trophic status and algal biomass in these lakes, yet this coupling appears to be system-specific and there does not appear to be a general relationship between algal biomass or productivity and OMP across lake types. The main pathways of OMP therefore remain unclear, and the contribution of different pathways may vary among lake types, which may explain the diversity of

OMP rates and potential drivers that have been reported in the literature. Our study extends the range of ecosystems where OMP has been detected, demonstrating that shallow lakes fit previously hypothesized morphometric relationships in terms of OMP contribution despite being highly eutrophic, and has established that phytoplankton does appear to play a major direct role in shaping ambient OMP rates.

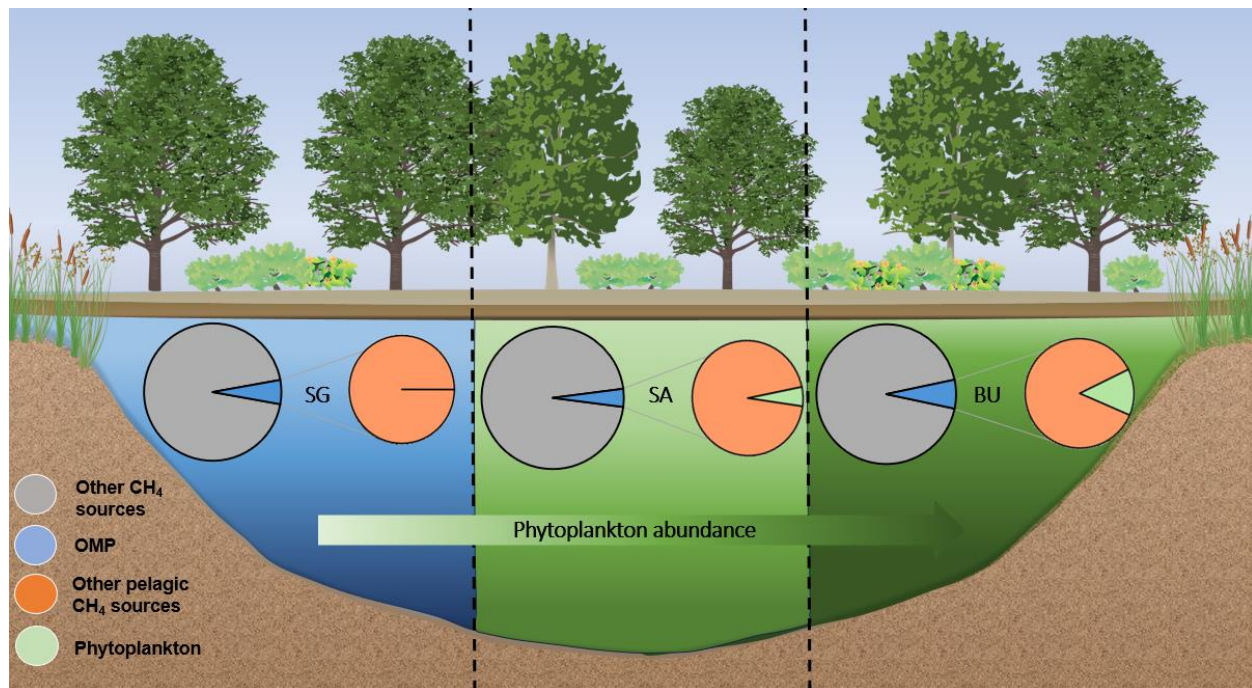


Figure 5. Conceptual figure depicting the contribution of OMP (blue) to total lake CH₄ diffusive flux (grey) and contribution of phytoplankton CH₄ production (green) to OMP ecosystem rates (orange), assuming the maximum potential scenario of contribution in all cases. *Tree and bush symbols from Dylan Taillie and Jane Hawkey, respectively, and emergent macrophyte symbols from Tracey Saxby, Integration and Application Network, University of Maryland Center for Environmental Science.*

Data availability

The data that support the findings of this study are available from the corresponding author upon reasonable request.

Funding

Préstamo BID PICT RAICES 2017-2498, Préstamo BID PICT 2015-1509, NSERC/HQ CarBBAS Industrial Research Chair, Society of Limnology (Tonolli prize) and Ministry of Education of Argentina alongside the German Academic Exchange Service (DAAD) (ALEARG fellowship).

References

- Conrad, R. Microbial Ecology of Methanogens and Methanotrophs. *Adv. Agron.* **96**, 1–63 (2007).
- Karl, D. M. *et al.* Aerobic production of methane in the sea. *Nat. Geosci.* **1**, 473–478 (2008).

- 629 3. Damm, E. *et al.* Methane production in aerobic oligotrophic surface water in the central Arctic
630 Ocean. *Biogeosciences* **7**, 1099–1108 (2010).
- 631 4. Grossart, H. P., Frindte, K., Dziallas, C., Eckert, W. & Tang, K. W. Microbial methane production in
632 oxygenated water column of an oligotrophic lake. *Proc. Natl. Acad. Sci. U. S. A.* **108**, 19657–
633 19661 (2011).
- 634 5. Tang, K. W., McGinnis, D. F., Frindte, K., Brüchert, V. & Grossart, H. P. Paradox reconsidered:
635 Methane oversaturation in well-oxygenated lake waters. *Limnol. Oceanogr.* **59**, 275–284 (2014).
- 636 6. Bižić-Ionescu, M., Ionescu, D., Günthel, M., Tang, K. W. & Grossart, H.-P. Oxic Methane Cycling:
637 New Evidence for Methane Formation in Oxic Lake Water. *Biog. Hydrocarb.* 379–400 (2019)
638 doi:10.1007/978-3-319-78108-2_10.
- 639 7. Perez-Coronel, E. & Michael Beman, J. Multiple sources of aerobic methane production in aquatic
640 ecosystems include bacterial photosynthesis. *Nat. Commun.* **13**, (2022).
- 641 8. Tang, K. W., McGinnis, D. F., Ionescu, D. & Grossart, H. P. Methane production in oxic lake
642 waters potentially increases aquatic methane flux to air. *Environ. Sci. Technol. Lett.* **3**, 227–233
643 (2016).
- 644 9. DelSontro, T., del Giorgio, P. A. & Prairie, Y. T. No Longer a Paradox: The Interaction Between
645 Physical Transport and Biological Processes Explains the Spatial Distribution of Surface Water
646 Methane Within and Across Lakes. *Ecosystems* **21**, 1073–1087 (2018).
- 647 10. Repeta, D. J. *et al.* Marine methane paradox explained by bacterial degradation of dissolved
648 organic matter. *Nat. Geosci.* **9**, 884–887 (2016).
- 649 11. Teikari, J. E. *et al.* Strains of the toxic and bloom-forming *Nodularia spumigena* (cyanobacteria)
650 can degrade methylphosphonate and release methane. *ISME J.* **12**, 1619–1630 (2018).
- 651 12. Yao, M., Henny, C. & Maresca, J. A. Freshwater bacteria release methane as a by-product of
652 phosphorus acquisition. *Appl. Environ. Microbiol.* **82**, 6994–7003 (2016).
- 653 13. Wang, Q., Dore, J. E. & McDermott, T. R. Methylphosphonate metabolism by *Pseudomonas* sp.
654 populations contributes to the methane oversaturation paradox in an oxic freshwater lake. *Environ.*
655 *Microbiol.* **19**, 2366–2378 (2017).
- 656 14. Peoples, L. M. *et al.* Oxic methane production from methylphosphonate in a large oligotrophic
657 lake: limitation by substrate and organic carbon supply. *Appl. Environ. Microbiol.* **89**, (2023).
- 658 15. Bižić-Ionescu, M., Ionescu, D., Günthel, M., Tang, K.W., Grossart, H. Oxic Methane Cycling: New
659 Evidence for Methane Formation in Oxic Lake Water. in *Biogenesis of Hydrocarbons* 1–22

- (Springer International Publishing, 2018). doi:https://doi.org/10.1007/978-3-319-53114-4_10-1.
16. Ernst, L. *et al.* Methane formation driven by reactive oxygen species across all living organisms. *Nature* **603**, 482–487 (2022).
 17. Bizic, M. Phytoplankton photosynthesis: An unexplored source of biogenic methane emission from oxic environments. *J. Plankton Res.* **43**, 822–830 (2021).
 18. Mao, Y. *et al.* Aerobic methane production by phytoplankton as an important methane source of aquatic ecosystems: Reconsidering the global methane budget. *Sci. Total Environ.* **907**, 167864 (2024).
 19. Batista, A. M. M., Woodhouse, J. N., Grossart, H. P. & Giani, A. Methanogenic archaea associated to *Microcystis* sp. in field samples and in culture. *Hydrobiologia* **831**, 163–172 (2019).
 20. Bogard, M. J. *et al.* Oxic water column methanogenesis as a major component of aquatic CH₄ fluxes. *Nat. Commun.* **5**, (2014).
 21. Günthel, M. *et al.* Photosynthesis-driven methane production in oxic lake water as an important contributor to methane emission. *Limnol. Oceanogr.* **65**, 2853–2865 (2020).
 22. Hartmann, J. F. *et al.* High Spatiotemporal Dynamics of Methane Production and Emission in Oxic Surface Water. *Environ. Sci. Technol.* **54**, 1451–1463 (2020).
 23. Morana, C. *et al.* Methane paradox in tropical lakes? Sedimentary fluxes rather than pelagic production in oxic conditions sustain methanotrophy and emissions to the atmosphere. *Biogeosciences* **17**, 5209–5221 (2020).
 24. Bižić, M. *et al.* Aquatic and terrestrial cyanobacteria produce methane. *Sci. Adv.* **6**, (2020).
 25. Klintzsch, T. *et al.* Stable Carbon Isotope Signature of Methane Released from Phytoplankton. *Geophys. Res. Lett.* (2023).
 26. Lenhart, K. *et al.* Evidence for methane production by marine algae (*Emiliana huxleyi*) and its implication for the methane paradox in oxic waters. *Biogeosciences Discuss.* **12**, 20323–20360 (2015).
 27. Klintzsch, T. *et al.* Methane production by three widespread marine phytoplankton species: Release rates, precursor compounds, and potential relevance for the environment. *Biogeosciences* **16**, 4129–4144 (2019).
 28. Klintzsch, T. *et al.* Effects of Temperature and Light on Methane Production of Widespread Marine Phytoplankton. *J. Geophys. Res. Biogeosciences* **125**, (2020).
 29. Donis, D. *et al.* Full-scale evaluation of methane production under oxic conditions in a mesotrophic

- lake. *Nat. Commun.* **8**, 1–11 (2017).
30. Schroll, M., Liu, L., Einzmann, T., Keppler, F. & Grossart, H. P. Methane accumulation and its potential precursor compounds in the oxic surface water layer of two contrasting stratified lakes. *Sci. Total Environ.* **903**, 166205 (2023).
31. Günthel, M. *et al.* Contribution of oxic methane production to surface methane emission in lakes and its global importance. *Nat. Commun.* **10**, 1–10 (2019).
32. Thottathil, S. D., Reis, P. C. J. & Prairie, Y. T. Magnitude and Drivers of Oxic Methane Production in Small Temperate Lakes. *Environ. Sci. Technol.* **56**, 11041–11050 (2022).
33. Liu, L. *et al.* Strong Subseasonal Variability of Oxic Methane Production Challenges Methane Budgeting in Freshwater Lakes. *Environ. Sci. Technol.* (2024) doi:10.1021/acs.est.4c07413.
34. Whiticar, M. J. Carbon and hydrogen isotope systematics of bacterial formation and oxidation of methane. *Chem. Geol.* **161**, 291–314 (1999).
35. Taenzer, L. *et al.* Low $\Delta^{12}\text{CH}_2\text{D}_2$ values in microbialgenic methane result from combinatorial isotope effects. *Geochim. Cosmochim. Acta* **285**, 225–236 (2020).
36. Baliña, S., Sánchez, M. L., Izaguirre, I. & del Giorgio, P. A. Shallow lakes under alternative states differ in the dominant greenhouse gas emission pathways. *Limnol. Oceanogr.* **68**, 1–13 (2022).
37. Izaguirre, I. *et al.* Which environmental factors trigger the dominance of phytoplankton species across a moisture gradient of shallow lakes? *Hydrobiologia* **752**, 47–64 (2015).
38. Baliña, S., Sánchez, M. L. & del Giorgio, P. A. Physical Factors and Microbubble Formation Explain Differences in CH_4 Dynamics Between Shallow Lakes Under Alternative States. *Front. Environ. Sci.* **10**, 1–11 (2022).
39. Soued, C. & Prairie, Y. T. The carbon footprint of a Malaysian tropical reservoir: measured versus modelled estimates highlight the underestimated key role of downstream processes. *Biogeosciences* **17**, 515–527 (2020).
40. Koschorreck, M., Prairie, Y. T., Kim, J. & Marcé, R. Technical note: CO_2 is not like CH_4 - Limits of and corrections to the headspace method to analyse pCO_2 in fresh water. *Biogeosciences* **18**, 1619–1627 (2021).
41. Knox, M., Quay, P. D. & Wilbur, D. Kinetic isotopic fractionation during air-water gas transfer of O_2 , N_2 , CH_4 , and H_2 . *J. Geophys. Res.* **97**, (1992).
42. Rippka, R. & Herdman, H. *Pasteur Culture Collection of Cyanobacterial Strains in Axenic Culture*. (Institut Pasteur, France, 1992).

- 722 43. Bischoff, H.W., Bold, H. C. Some soil algae from Enchanted Rock and related algal specie. in
723 *Phycological Studies IV* vol. IV 1–95 (Univ. Texas Publ., Austin - Texas, USA, Texas, 1963).
- 724 44. Archibald, P. A., & Bold, H. C. *Phycological Studies*. (Univ. Texas Public, 1970).
- 725 45. Komárek, J., & Anagnostidis, K. *Süsswasserflora von Mitteleuropa. Cyanoprokaryota 1.*
726 *Chroococcales*. (Gustav Fischer, Jena., 1999).
- 727 46. Komárek, J. *Cyanoprokaryota 2. Teil/2nd Part: Oscillatoriales. Susswasserflora von Mitteleuropa*
728 (2005).
- 729 47. Komárek, J. *Chlorophyceae (Grünalgen) Ordnung Chlorococcales*. (1983).
- 730 48. Ordóñez, C. *et al.* Evaluation of the methane paradox in four adjacent pre-alpine lakes across a
731 trophic gradient. *Nat. Commun.* **14**, 2165 (2023).
- 732 49. Encinas Fernández, J., Peeters, F. & Hofmann, H. On the methane paradox: Transport from
733 shallow water zones rather than in situ methanogenesis is the major source of CH₄ in the open
734 surface water of lakes. *J. Geophys. Res. Biogeosciences* **121**, 2717–2726 (2016).
- 735 50. Peeters, F., Encinas Fernandez, J. & Hofmann, H. Sediment fluxes rather than oxic
736 methanogenesis explain diffusive CH₄ emissions from lakes and reservoirs. *Sci. Rep.* **9**, 1–10
737 (2019).
- 738 51. Peeters, F. & Hofmann, H. Oxic methanogenesis is only a minor source of lake-wide diffusive CH₄
739 emissions from lakes. *Nat. Commun.* **12**, (2021).
- 740 52. Sánchez, M. L., Lagomarsino, L., Allende, L. & Izaguirre, I. Changes in the phytoplankton structure
741 in a Pampean shallow lake in the transition from a clear to a turbid regime. *Hydrobiologia* **752**, 65–
742 76 (2015).
- 743 53. Murase, J. & Sugimoto, A. Inhibitory effect of light on methane oxidation in the pelagic water
744 column of a mesotrophic lake (Lake Biwa, Japan). *Limnol. Oceanogr.* **50**, 1339–1343 (2005).
- 745 54. Shelley, F., Ings, N., Hildrew, A. G., Trimmer, M. & Grey, J. Bringing methanotrophy in rivers out of
746 the shadows. *Limnol. Oceanogr.* **62**, 2345–2359 (2017).
- 747 55. Thottathil, S. D., Reis, P. C. J., del Giorgio, P. A. & Prairie, Y. T. The Extent and Regulation of
748 Summer Methane Oxidation in Northern Lakes. *J. Geophys. Res. Biogeosciences* **123**, 3216–
749 3230 (2018).
- 750 56. Oswald, K. *et al.* Light-dependent aerobic methane oxidation reduces methane emissions from
751 seasonally stratified lakes. *PLoS One* **10**, 1–22 (2015).
- 752 57. Broman, E. *et al.* No evidence of light inhibition on aerobic methanotrophs in coastal sediments

using eDNA and eRNA. *Environ. DNA* **5**, 766–781 (2023).

58. Zhang, Y. & Xie, H. Photomineralization and photomethanification of dissolved organic matter in Saguenay River surface water. *Biogeosciences* **12**, 6823–6836 (2015).

59. Li, Y., Fichot, C. G., Geng, L., Scarratt, M. G. & Xie, H. The Contribution of Methane Photoproduction to the Oceanic Methane Paradox. *Geophys. Res. Lett.* **47**, 1–10 (2020).

Acknowledgements

We thank F. Zolezzi for assistance in the field, A. Parkes for support with laboratory work and logistics and D. Kachanovsky for ambiental DNA analysis support. We are also grateful to C. Soued, P. Reis and Y. Prairie for their valuable discussions and insights. We are grateful to the International Society of Limnology (SIL) for awarding the Tonolli Prize to S. Baliña, which funded a significant share of the mesocosm field experiments. We thank the Ministry of Education of Argentina and the German Academic Exchange Service (DAAD) for funding the ALEARG fellowship, which enabled S. Baliña to conduct the phytoplankton strain experiments in Germany. This work was also supported by the NSERC/HQ CarBBAS Industrial Research Chair, by Préstamo BID PICT RAICES 2017-2498 and by Préstamo BID PICT 2015-1509.

Author contribution statement

S.B. contributed substantially to the designing of the research, field work and data acquisition, phytoplankton strain's isolation and phytoplankton experiments, molecular analysis, statistical analyses and writing of the manuscript. M.L.S. contributed substantially to the designing of the research, field work and data acquisition. M.B, D. I and H. P. G contributed substantially to the phytoplankton experiments carried out in Germany. S.T. contribute substantially to the isotopic mass balances. M. C. B contribute substantially to field work and data acquisition. A. J contributed substantially to the isolation of phytoplankton strains. P.A.G. contributed substantially to the designing of the research, analyses of the results and writing of the manuscript. All authors reviewed the manuscript.

Supplementary information for:

**Oxic methane production in shallow productive lakes:
linking field and in vitro experimental evidence**

Sofía Baliña^{1*}, María Laura Sánchez¹, Mina Bizic², Danny Ionescu², Shoji D. Thottathil³, María Carolina Bernal¹, Angela Juárez⁴, Hans-Peter Grossart^{5,6}, Paul A. del Giorgio⁷

¹Laboratorio de Limnología, Departamento de Ecología, Genética y Evolución, Facultad de Ciencias Exactas y Naturales, Universidad de Buenos Aires, Instituto de Ecología, Genética y Evolución de Buenos Aires (IEGEBA - CONICET/UBA), Ciudad Autónoma de Buenos Aires, Argentina

²Chair of Environmental Microbiomics, Technische Universität Berlin, Berlin, Germany

³Department of Environmental Science and Engineering, SRM University AP, Amaravati, Andhra Pradesh 522 502, India.

⁴Universidad de Buenos Aires, Facultad de Ciencias Exactas y Naturales, Departamento de Biodiversidad y Biología Experimental and CONICET-Universidad de Buenos Aires, Instituto de Biodiversidad y Biología Experimental y Aplicada (IBBEA), Buenos Aires, Argentina.

⁵Leibniz Institute of Freshwater Ecology and Inland Fisheries (IGB), Alte Fischerhütte 2, D-16775 Stechlin, Germany.

⁶Institute of Biochemistry and Biology, Potsdam University, Maulbeerallee 2, D-16775 Stechlin, Germany

⁷Département des Sciences Biologiques, Université du Québec à Montréal, Montréal, Québec, Canadá

Contents:

- Figure S1: Study area map
- Figure S2: Pictures of the field setup
- Supplementary Information 1: Information about the polycarbonate used to build the mesocosms
- Table S1: Parameters sampled during the experiments
- Supplementary Information 2: Archaea and bacteria community composition
- Supplementary Information 3: Ecosystem metabolism calculations
- Supplementary Information 4: Details of diffusive flux measurements
- Supplementary Information 5: Details of exchange velocity calculations
- Figure S3: Mesocosm and lake temperature profiles
- Figure S4: Mesocosm and lake oxygen profiles
- Figure S5: Workflow and details employed to estimate methane oxidation rates
- Figure S6: Observed dissolved CH₄ concentrations in the mesocosms throughout the experiments
- Figure S7: MIMS setup and functioning
- Supplementary information 6: Details on Chla and DNA analyses for phytoplankton cultures
- Figure S8: Characterization of MIMS physical loss

- Figure S9: Phytoplankton community composition
- Figure S10: Methanogenic archaea & methanotrophic bacteria community composition: class level
- Figure S11: Observed CH₄ dissolved concentrations and ¹³C-CH₄ from the lake and the mesocosms
- Figure S12: CH₄ diffusive flux and K₆₀₀ CH₄ for lakes and mesocosms
- Figure S13: CH₄ dissolved, ¹³C-CH₄ and CO₂ dissolved, from dark MOX incubations
- Figure S14: Linear relationship between ln (dissolved CH₄) vs Time, from dark MOX incubations
- Figure S15: Expected standardized CH₄ concentrations (day⁻¹) for MOX, EVA and MOX+EVA curves
- Figure S16: Linear relationship between ln (dissolved CH₄) vs ln (¹³C-CH₄ + 1000) from MOX dark incubations
- Figure S17: MIMS measurement of milliq water and BG11
- Figure S18: Results from PCR to detect methanogenic archaea and methanotrophic bacteria
- Figure S19: Log₁₀(standardized OMP) vs log₁₀(Chla) including data from this and other studies

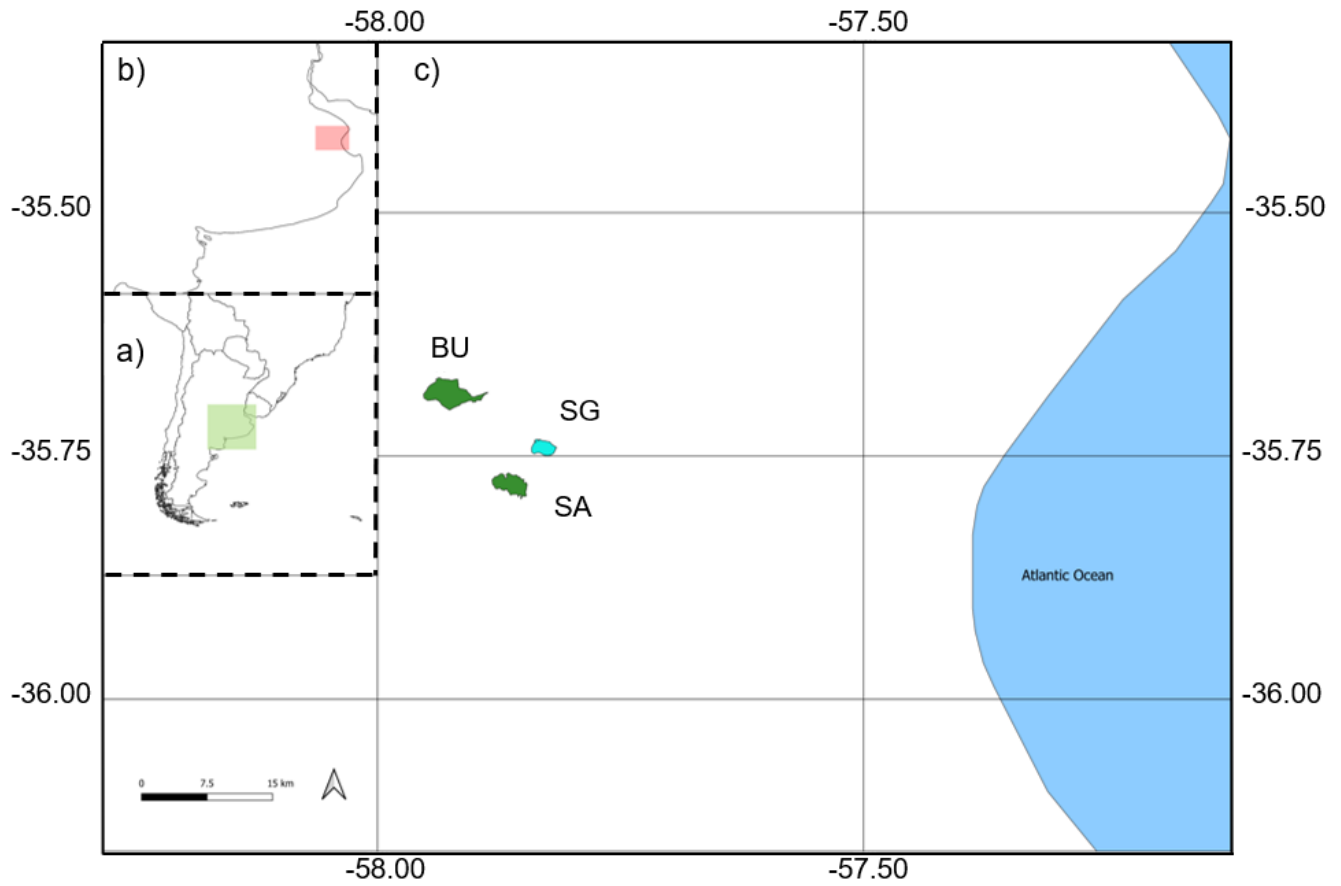


Figure S1. Study area map. a) the province of Buenos Aires, Argentina, is highlighted in green, b) the study area, within the province of Buenos Aires, is highlighted in red and c) the two turbid phytoplanktonic (SA and BU) and one clear vegetated (SG) shallow lakes analyzed in this study.



Figure S2. Pictures of the field setup in the three studied lakes (SG, SA and BU). The upper left picture has an inset showing the shower-like head and the 55µm pore size net. *Credits: M. Laura Sánchez and Sofia Baliña.*

Supplementary Information 1

The polycarbonate used to build the mesocosms was also used by Bogard et al., (2014) and tested for CH₄ passage through it: the membrane influx rate obtained was 0.0021 ± 0.0001 mmol CH₄ enclosure⁻¹ day⁻¹. Considering that those mesocosms had 4712 L, the rate was converted to the same units used in this study: 0.00044 ± 0.00002 μmol CH₄ L⁻¹ day⁻¹, a negligible amount.

Table S1. Sampling design description

Limnological parameters	Installation (T0)	24hs after T0	End of experiments	In between days
Secchi depth		✓	✓	
Turbidity		✓	✓	
TSS		✓	✓	
Irradiance profile		✓	✓	
pH	✓	✓	✓	✓
O ₂ and T° profile	✓	✓	✓	✓
TP and TN		✓	✓	
DOC and DIC		✓	✓	
Chla		✓	✓	
Phytoplankton		✓	✓	
Ambiental DNA		✓	✓	
Dissolved CO ₂ and CH ₄	✓	✓	✓	✓
¹³ C-CO ₂ and ¹³ C-CH ₄	✓	✓	✓	✓
CO ₂ and CH ₄ diffusive fluxes		✓	✓	
MOX dark incubations		✓		
Meteorological parameters	Installation (T0)	After 24hs of T0	End of the experiment	In between days
Air temperature	✓	✓	✓	✓
Air pressure	✓	✓	✓	✓
Humidity	✓	✓	✓	✓
Wind speed	✓	✓	✓	✓

O₂ (mg L⁻¹), T° (°C), Turbidity (NTU), Total Suspended Solids (TSS, mg L⁻¹), Total Phosphorus and Total Nitrogen (µg L⁻¹ and mg L⁻¹, respectively), Dissolved Organic Carbon (DOC, mg L⁻¹), Dissolved Inorganic Carbon (DIC, mg L⁻¹), Irradiance (µmol photons m⁻² s⁻¹), Chlorophyll a (Chla, µg L⁻¹), Phytoplankton (ind ml⁻¹), Pressure (mbar), Humidity (%), Wind speed (m s⁻¹).

Supplementary information 2

1. Ambiental molecular analysis

To explore the archaea and bacteria communities, ambiental DNA samples were taken from the lake and from the mesocosms at the beginning and at end of the experiment (Table. S1). DNA was extracted and sequences with specific primers for archaea and bacteria.

1.1. DNA extraction & sequencing

DNA extraction was carried out following Fernández Zenoff (et al., 2006). To extract ambiental DNA, water was filtered through 0.2µm filters (Millipore®) and the filters were preserved at -80°C until DNA extraction. A protocol including chloroform: ethanol was used: Chloroform: ethanol protocol: 0.75mL of buffer CTAB lysis buffers were added to half of the filter and incubated 30' at 60°C. After, 0.7mL of isoamyl: chloroform were added and mixed by inversion, following a centrifugation step of 10' at 14.000 rpm. The aqueous phase was transferred to another eppendorf. The isoamyl: chloroform step was repeated two more times. To the final aqueous phase obtained, the same volume of isopropanol was added, following an incubation of 1 hour at 4°C. Afterwards, a centrifugate step for 30' at 14.000 rpm was done. The obtained pellet was washed with cold Ethanol 80%. We let the pellet completely dry and then resuspended in 20µl of miliq sterilized water. DNA concentration (ng µl⁻¹) of each sample was measured using a Nanodrop®. DNA samples were sent to *plateforme de génomique* CERMO-FC, Université du Québec à Montréal, for paired-end sequencing of the 16S rRNA V4 region using the primers A340F (5'-CCC TAC GGG GYG CAS CAG-3') and 915R (5'-GTG CTC CCC CGC CAA TTC CT-3') for archaea, and the primers 515F (5'-GTGCCAGCMGCCGCGGTAA-3') and 806R (5'-GGACTACHVGGGTWTCTAAT-3') for bacteria. A Miseq platform (PE250, Illumina, San Diego, CA, USA) was used.

1.2. Bioinformatic analysis

The obtained sequences were processed using the DADA2 package in the R environment (Callahan et al., 2016). Bioinformatic processing was carried out for bacteria and archaea separately. In each case processing involved the following steps: 1) Quality sequence plots were generated and inspected for each of the samples; 2) Raw sequences were trimmed and filtered using the filterAndTrim function with the following parameters: truncQ = 2, rm.phix = TRUE, trimleft = corresponding to primer size in each case, trunLen = nothing for archaea and 240pb and 170pb for forward and reverse sequences, respectively, for bacteria. For archaea sequences were not trimmed because the amplicons were long and trimming would have prevented sequence reads from overlapping and, therefore, making contig construction impossible; 3) Sequencing error models were generated for the samples, for forward and reverse reads separately, using the learnErrors function; 4) Unique sequence groups were determined for forward and reverse reads, considering the error model generated in the previous step. A dataframe containing the abundance of each unique sequence detected was generated; 5) Amplicons were generated by merging the forward and reverse sequences, with a minimum overlap of 12 nucleotides and a maximum of zero mismatches; 6) ASV (amplicon sequence variant) tables were constructed with sequences and abundances for each sample; 7) Chimeras were detected and removed, considering that an amplicon is considered a chimera if it can be reconstructed from the forward and reverse parts of amplicons that are at least 1.5 times more abundant; 8)

Taxonomic assignment was performed for each detected ASV using the `assignTaxonomy` and `addSpecies` function of the DADA2 package. The first case reaches genus level, while the second one reaches species level. In all cases, version 132 of the SILVA database was used. The ASV table obtained was filtered to remove undesired assignments, such as chloroplasts, mitochondria, eukaryotes in the bacteria dataset and bacteria in the archaea dataset. Finally, only ASVs with more than 10 reads and present in at least two samples were retained. The final ASV set consisted of 4343 ASV for bacteria and 1969 ASV for archaea. Subsequently, the samples were normalized to the minimum number of reads in a sample (Cmin) using the SRS workflow, which aims to preserve the relative abundance of ASV as closely as possible to the original dataset. Descriptive analyses of the ASV table were conducted using the Phyloseq and Biostrings package.

Supplementary information 3

Gross primary production (GPP), ecosystem respiration (ER), and net ecosystem production (NEP) rates were calculated following Soued & Prairie (2021), by means of high-frequency data obtained with O₂ and temperature sensors (miniDO₂T, Precision Measurement Engineering, Inc.®) that were deployed in the lake and the mesocosms. Ecosystem metabolism rates were calculated based on a diurnal open system O₂ model (ODUM, 1956), in which changes in O₂ concentration are a function of GPP, ER, and O₂ exchange at the water-air interface (K_{O2}), following equation S1.

Ecosystem metabolism rates were calculated based on a diurnal open system O₂ model (Odum 1956), in which changes in O₂ concentration are a function of GPP, ER, and O₂ exchange at the water-air interface (K_{O2}), following equation S1.

$$\frac{dO_2}{dt} = \frac{GPP}{Z_{epi}} + \frac{ER}{Z_{epi}} + K_{O_2}(O_{2\ sat} - O_2) \quad eq.S1$$

Where Z_{epi} is the epilimnion depth, which in our case is the depth of the mesocosm (0.8m). $O_{2\ sat}$ is the theoretical concentration of O₂ at saturation, considering the in-situ temperature and atmospheric pressure. O_2 is the empirically measured oxygen concentration in the water. Detailed equations of the model can be found in Hall & Hotchkiss (2017).

Estimates of GPP and ER were obtained through maximum likelihood using equation S1 and the R package Stream Metabolizer (Appling et al., 2018). Net primary production (NPP) was then calculated as GPP - ER. A value for GPP, ER, and NPP was obtained for each day in each case. For the lake, a daily average of each parameter was calculated from the single sensor placed, so the variability associated with this mean corresponds to the day-to-day variation within that same sensor. For the mesocosms, a daily average was calculated for each mesocosm, and then the mean value of all these averages was determined, so the deviation between these data points reflects the variability among mesocosms.

Supplementary information 4

CO₂ and CH₄ diffusive fluxes between the air: water interface were measured by means of an opaque floating chamber, following Baliña et al., (2022). The air inside the chamber was sampled every 5' during 15', obtaining a total of four time points. Samples were injected in 30mL glass pre-evacuated vials equipped with crimped rubber stoppers (Exetainer, Labco) and analyzed in a cavity ringdown spectrometer (Picarro G2201-i). The diffusive flux rates (f_{gas}) were calculated in mmol m⁻² d⁻¹, following equation S2. All chamber measurements were performed between 7am and 7pm.

$$f_{gas} = \left(\frac{s \cdot V}{mV \cdot A} \right) * t \quad eq.S2$$

Where s is the accumulation rate of gas in the chamber (ppm min⁻¹); V is the volume of the chamber (L); A is the chamber surface area (m²); mV is the molar volume of the gas at ambient temperature and pressure (L mmol⁻¹); and t is a factor that converts minutes to days (1 day = 1440 min) (DeSontro et al., 2016).

Supplementary information 5

Exchange velocities (K) were calculated using the data from GHG dissolved and diffusive fluxes, following Baliña, Sánchez, & del Giorgio (2022) (equation S3).

$$K = \frac{Flux\ gas}{Kh * \Delta p_{Gas}} \quad eq. S3$$

Where Flux gas is the diffusive flux for CH₄ or CO₂ obtained from Eq. x (mmol m⁻² d⁻¹), Kh is the Henry's constant correspondent corrected for atmospheric pressure and water temperature, and Δp_{Gas} is the difference between the partial pressure of the gas in the water (P_w) and the partial pressure of the gas in equilibrium with the atmosphere (P_{eq}), i.e. Δp_{Gas} (ppmv) = P_w - P_{eq}.

The obtained values of K were standardized to a Schmidt number of 600 (eq. x), obtaining the standardized K₆₀₀ (equation S4).

$$K_{600} = \frac{K_{CO2\ or\ CH4}}{(Sc_{CO2\ or\ CH4}/600)^{-n}} \quad eq. S4$$

Where Sc is the Schmidt number of a given gas at a given temperature (Wanninkhof, 1992), and n is a value that depends on wind speed. We used a value of n = 2/3 for ambient wind speeds <3.7 m s⁻¹ and of n = 1/2 for ambient wind speeds >3.7 m s⁻¹ (Guérin et al., 2007).

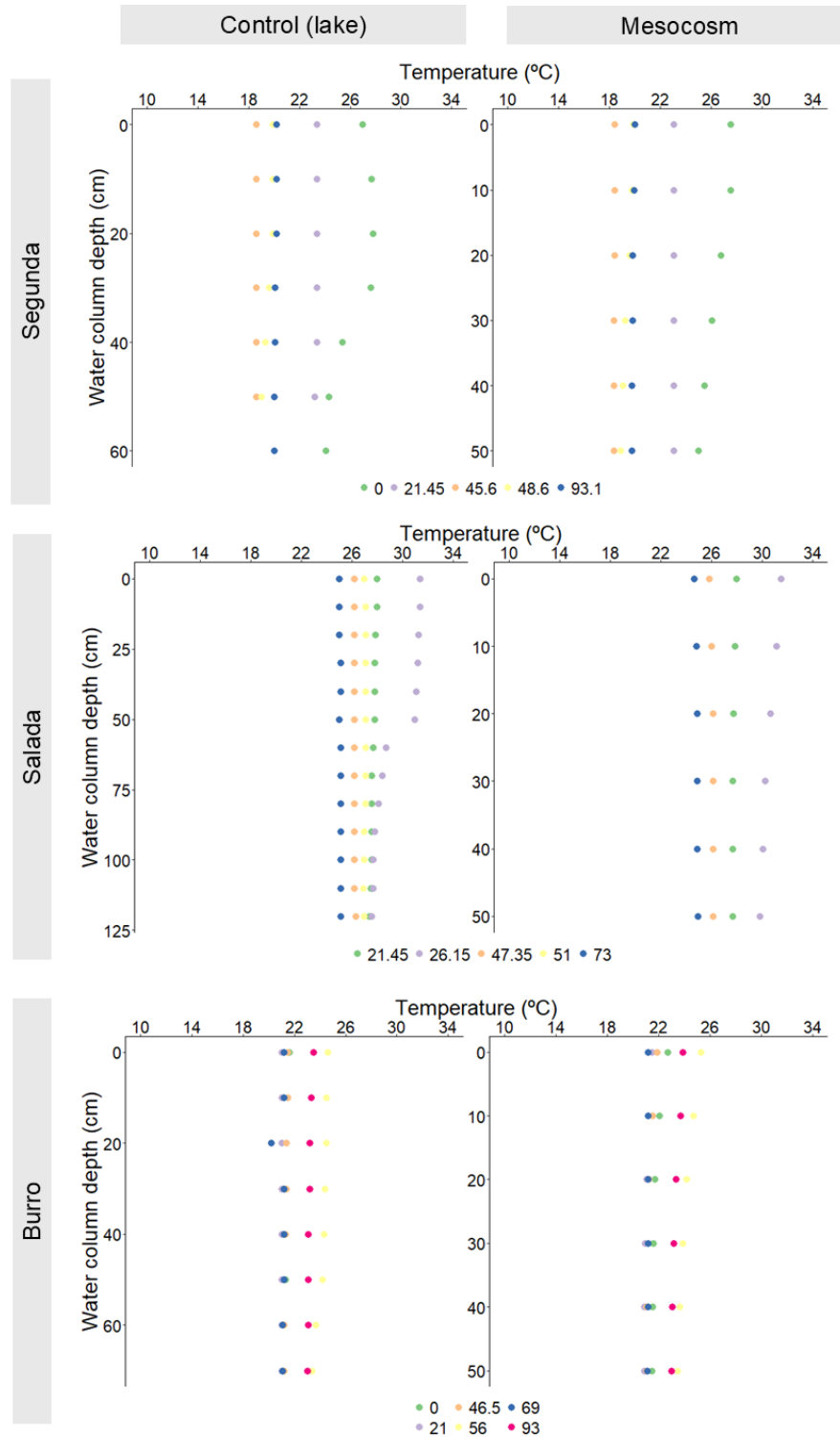


Figure S3. Temperature profiles for the lake (Control, C) and the mesocosms (M). Each color represents a different time during the experiment. Temperature values for the lake correspond to one measurement *per* time, whereas temperature values for the mesocosm correspond to an average of all temperature measurements *per* time across all mesocosms.

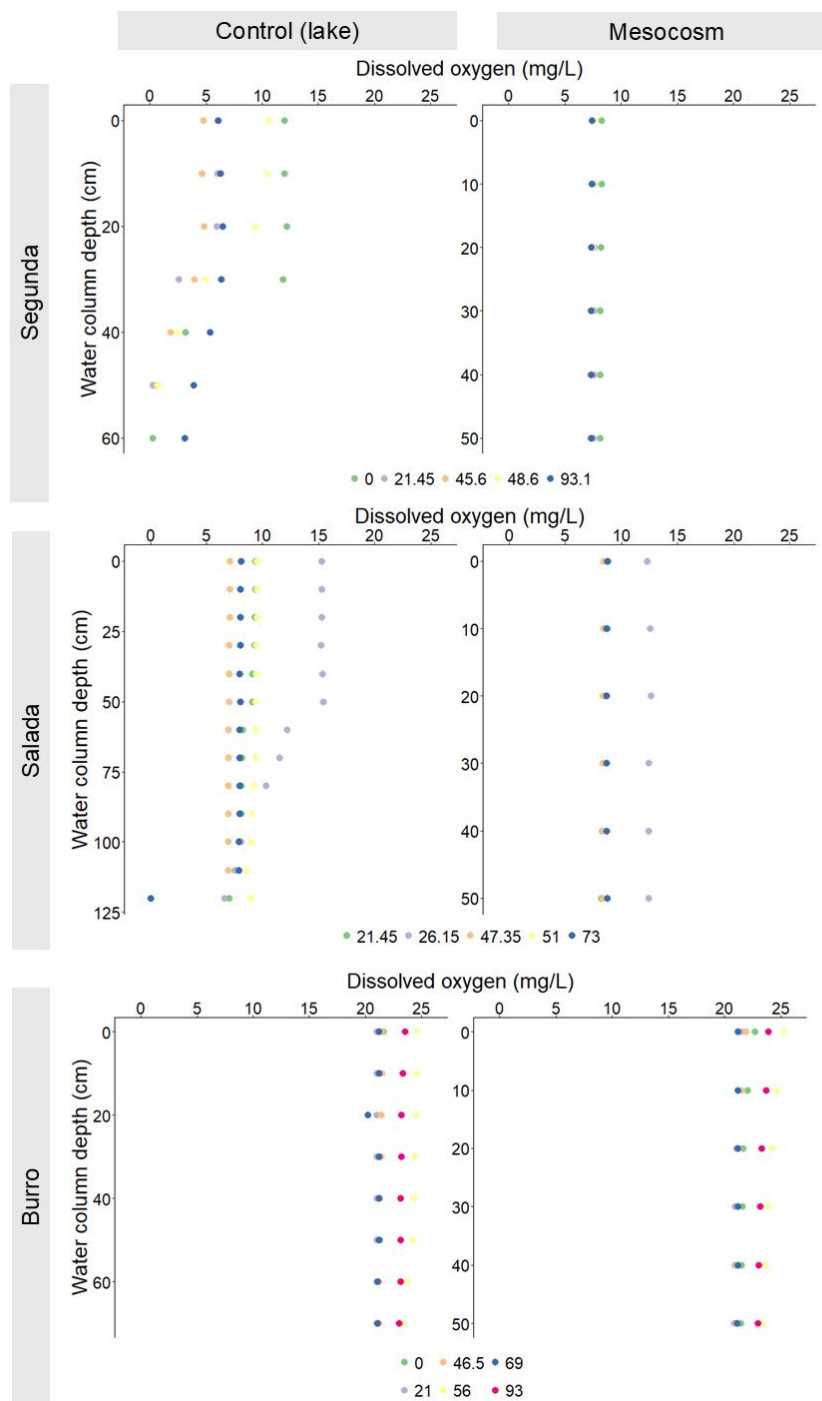


Figure S4. Dissolved oxygen profiles for the lake (Control, C) and the mesocosms (M). Each color represents a different time during the experiment. Dissolved oxygen values for the lake correspond to one measurement *per* time, whereas values for the mesocosm correspond to an average of all measurements *per* time across all mesocosms.

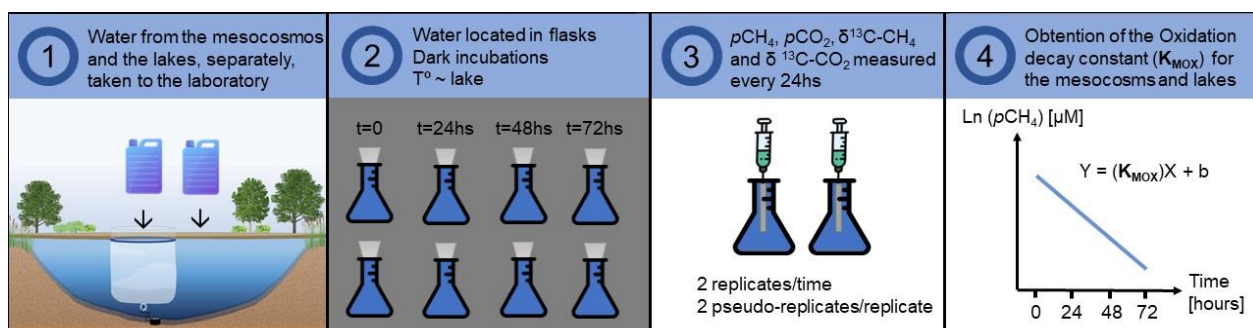


Figure S5. Workflow employed to estimate methane oxidation rates (MOX) and to derive the oxidation decay constant (K_{MOX}) for the mesocosms (treatment) and lakes (control). 1) A 5 L cubitainer was filled with water from the lake and another with water from all the mesocosms in equal proportions, no later than 24 h after the initial deployment of the mesocosms, and without leaving any headspace. 2) In the laboratory, eight 500 mL erlenmeyers flasks were filled from each cubitainer, without leaving any headspace. The flasks were firmly sealed with a silicone stopper and tape to avoid any exchange with the atmosphere. Each set of eight flasks was placed in different incubators at ambient temperature. 3) Immediately after preparing the setup, samples to measure the concentration of dissolved CH_4 and CO_2 , along with $^{13}\text{C-CH}_4$ and $^{13}\text{C-CO}_2$, were taken in duplicate from two of the eight flasks from each incubator using the headspace technique, as described in section 4.1. These measurements were considered time zero. After this initial time point, each pair of flasks were sampled in duplicate every 24 h, up to 72 h. 4) Since MOX follows first order kinetics, the instantaneous CH_4 oxidation rate (h^{-1}) for each lake or mesocosm can be obtained as the slope of the regression between $\ln(\text{dissolved CH}_4)$ (μM) vs Time (h) (Thottathil et al., 2022). This estimate of oxidation decay constant (K_{MOX}) was used for the mesocosm CH_4 mass balances calculations.

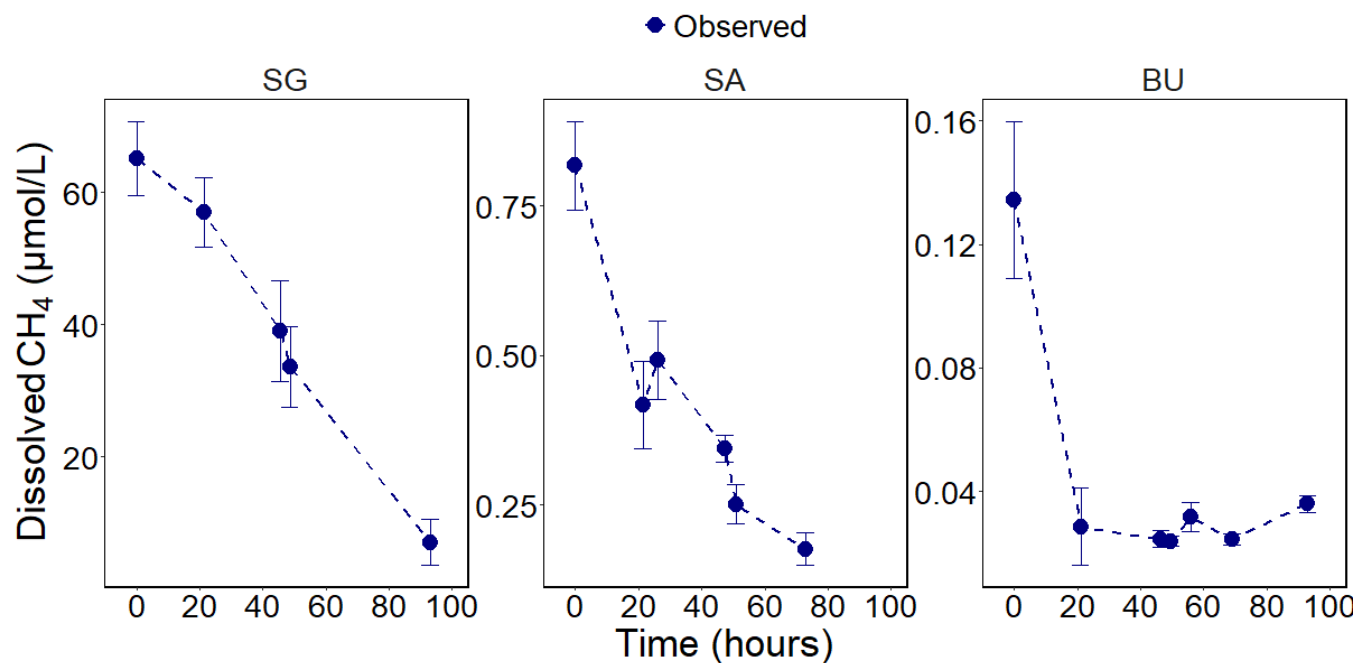


Figure S6. Dissolved CH_4 in the mesocosms of Segunda (SG), Salada (SA) and El Burro (BU), throughout the field experimental time. Each data point corresponds to an average of all measurements *per* time across all mesocosms, whereas the bar indicates the standard deviation.

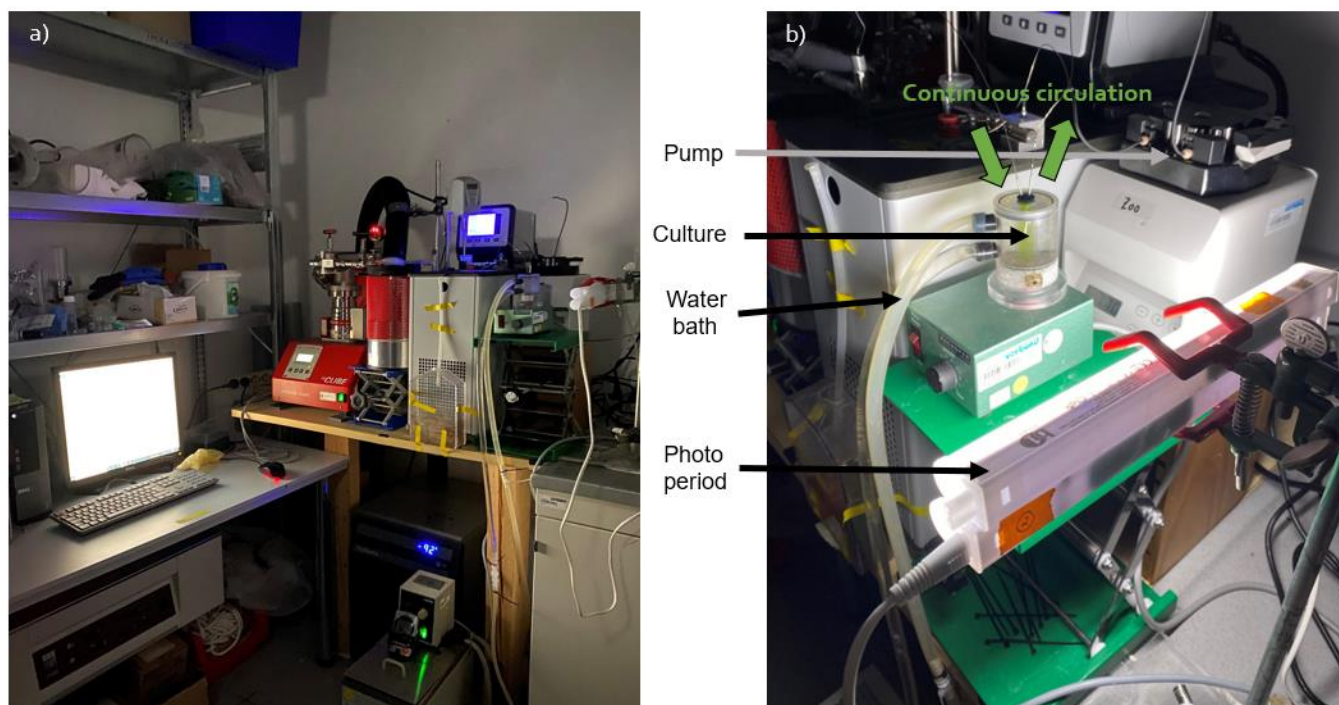


Figure S7. Membrane Inlet Mass Spectrometer (MIMS) setup. a) general experimental setup, b) details of the culture setup. The experiments were conducted using a MIMS (Bay Instruments, MD, USA), which consists of a Pfeiffer Vacuum HiCube 80 Eco Turbo pumping station connected to a crossed-beam ion source mass spectrometer QMG 220 M1, PrismaPlus, C-SEM, (Pfeiffer Vacuum, Germany). This type of mass spectrometer features a semi-permeable, thin and hydrophobic membrane that is useful to measure small and nonpolar molecules, such as O_2 and CH_4 . Therefore, it is particularly useful for measuring the concentrations of these two gasses dissolved in liquid samples, such as a culture. Each measured culture was placed in a 3.5 ml chamber surrounded by an outer chamber filled with water, connected to a thermostatic bath for temperature control. The culture chamber is equipped with a magnetic stirrer at the bottom to prevent concentration gradients and was exposed to a photoperiod of 15 hours of light and 9 hours of darkness (the same as used for acclimating the cultures). At its upper end, the culture chamber has two steel capillary tubes: one of them takes culture and sends it to the mass spectrometer for measurement, while the other returns the measured culture to the chamber, creating a closed system for the liquid. This circuit is achieved by a peristaltic pump (Minipuls 3, Gilson). The culture taken from the culture chamber through the capillary comes into contact with the thin, semi-permeable membrane (8 mm long microbore silicone membrane, Silastic, DuPont) through which they pass through and are collected in another tube. This collecting tube then passes through a cold trap to freeze any remaining liquid and prevent it from entering the MIMS. Once past this point, the gases enter the MIMS, where molecules are ionized, accelerated by an electric field, deflected by a magnetic field, and finally collected by a detector (Burlacot et al., 2020). This measurement is performed every 12 seconds. It is important to note that this system creates a closed circuit for liquids but not for gases, resulting in a constant physical loss of gases to the atmosphere.

Supplementary information 6

To measure Chla the protocol from Strickland, J. D. H., & Parson (1965) was followed. A volume between 1 and 2.5 ml (depending on if it was the onset or offset of the experiment) was filtered through a 2.5 cm GF/C glass fiber filter (Whatman). These filters were kept under -20°C until determination. Upon Chla extraction, each filter was located in a glass-stoppered centrifuge tube and 10mL of acetone 90% were added. These tubes were left 24hs at 4°C, under complete darkness. On the following day, Chla and phaeophytin concentrations were measured using a Hitachi Spectrometer 2900. The emission spectra of Chla fluorescence were measured in the wavelengths of 630, 645, 665 and 750 λ , whereas the emissions spectra of phaeophytin was measured in the wavelengths of 665 and 750 λ . Calculations of the amount of Chla followed by Lorenzen (1967).

For DNA extraction, a volume between 1 and 3 ml (depending on if it was the onset or offset of the experiment) were filtered through 0.2 μ filters (Millipore®). These filters were kept under -20°C. Upon DNA extraction, the protocol from Nercessian et al. (2005) was followed. After DNA extraction, PCR was carried out using specific primers for methanogenic archaea and methanotrophic bacteria. To detect archaea primers for the *mcrA* gene were used (*mlas* - *modF* 5'-GGYGGTGTMGDDTTCACMCARTA-3', *mcrA* 5'-CGTTCATBGCGTAGTTVGGRTAGT-3', product of ~450nt), which codifies for a subunit of the methyl coenzyme reductase M, related with methanogenesis and therefore biomarker of methanogenic archaea (Conrad 2005). To detect methanotrophic bacteria primers for the *pmoA* gene were used (*A189F* 5'-GGNGACTGGGACTTCTGG-3', *mb661R* 5'-CCGGMGCAACGTCYTTACC-3'), which codifies for a subunit of the pMMO enzyme, related with methane oxidation and therefore biomarker of methanotrophic bacteria (Samad & Bertilsson, 2017). For all of the PCR a HotStarTaq Plus Master Mix Kit (Qiagen, USA) was used. Please refer to Suppl. Inf. 6 for the details of the PCRs carried out. For the *mcrA* gene the PCR had the following conditions: 94°C for 3 min, followed by 30 cycles of 94°C for 30s, 55°C for 30s y 72°C for 30s, after which there was a final elongation step of 5min at 72°C. For the *pmoA* gene the PCR had the following conditions: 94°C for 3 min, followed by 40 cycles of 94°C for 1min, 55°C for 1min y 72°C for 1min, after which there was a final elongation step of 5min at 72°C. After amplification, PCR products were tested with an agarose gel 2% to determine if amplification was successful and if there were archaea/bacteria in each of the samples. As a positive control for archaea and bacteria, known positive PCR products of methanogenic archaea and methanotrophic bacteria where used, whereas the master mix of the PCR without sample was used as a negative control.

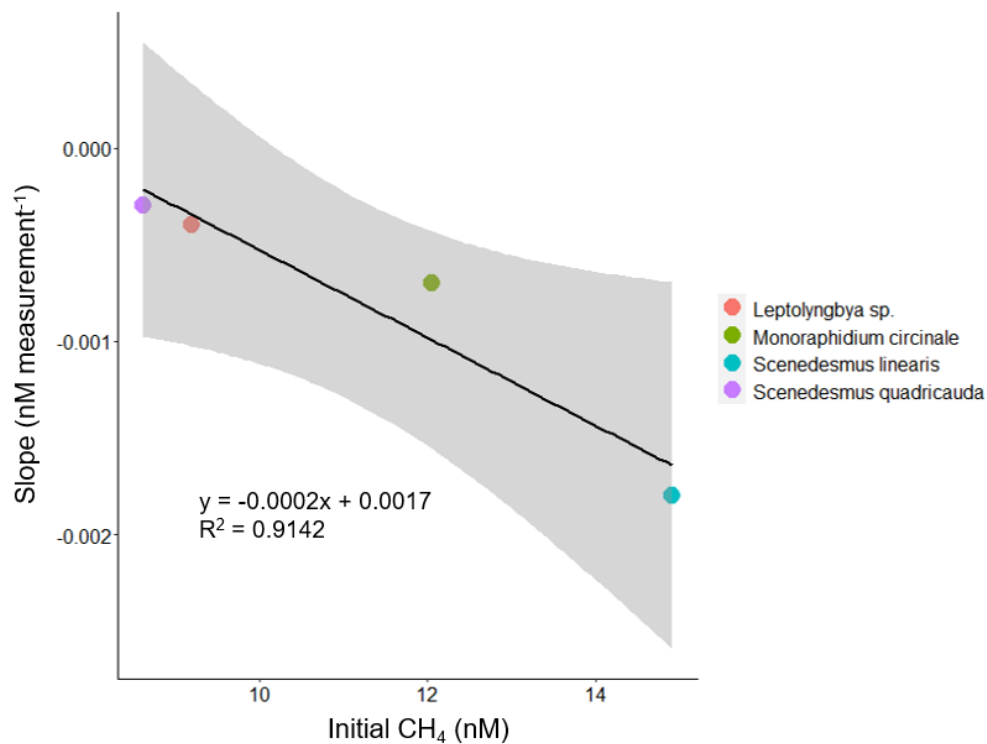


Figure S8. Characterization of MIMS physical loss. The Y axis corresponds to the slope of the regression between CH₄ (nM) and each measurement for each autoclaved culture, whereas the X axis corresponds to the initial CH₄ concentration of that same autoclaved culture (nM). The four points correspond to the autoclaved cultures of *Monoraphidium circinale*, *Scenedesmus linearis*, *Scenedesmus quadricauda* and *Planktolyngbya* sp. The rest of the tested isolated strains were not autoclaved, the ones presented here were used as a subset.

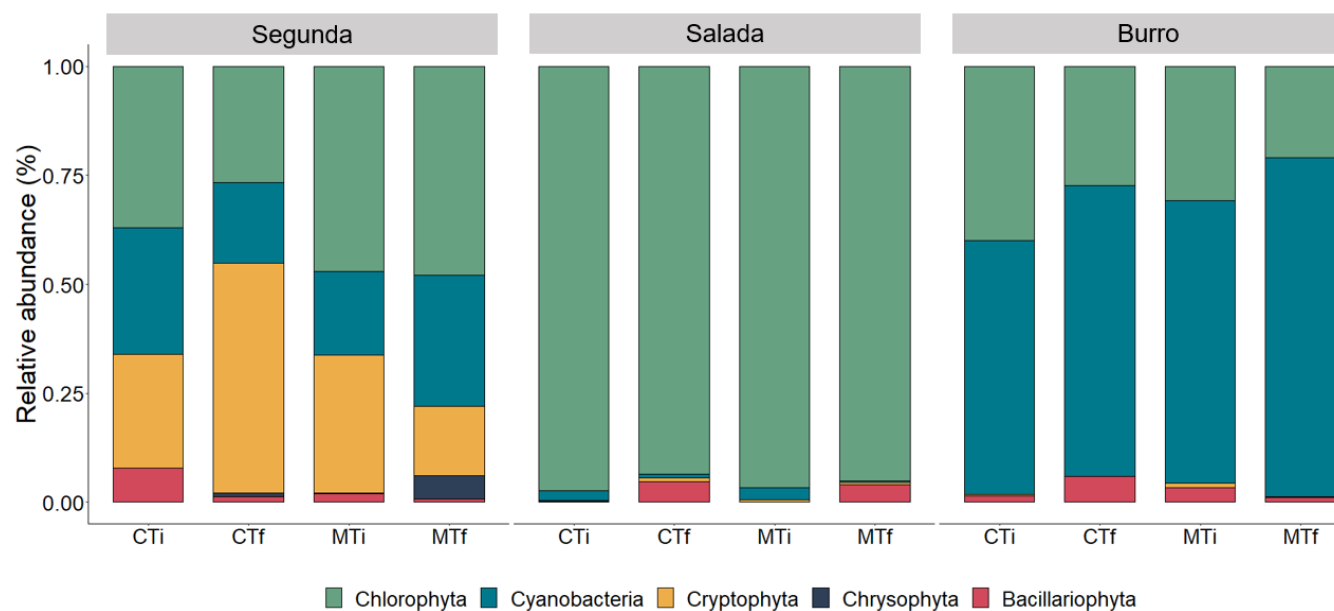


Figure S9. Phytoplankton community relative abundance for the lake (C) and the mesocosms (M) at the onset (T0) and end (TF) of each experiment. The phytoplanktonic groups are differentiated by colors.

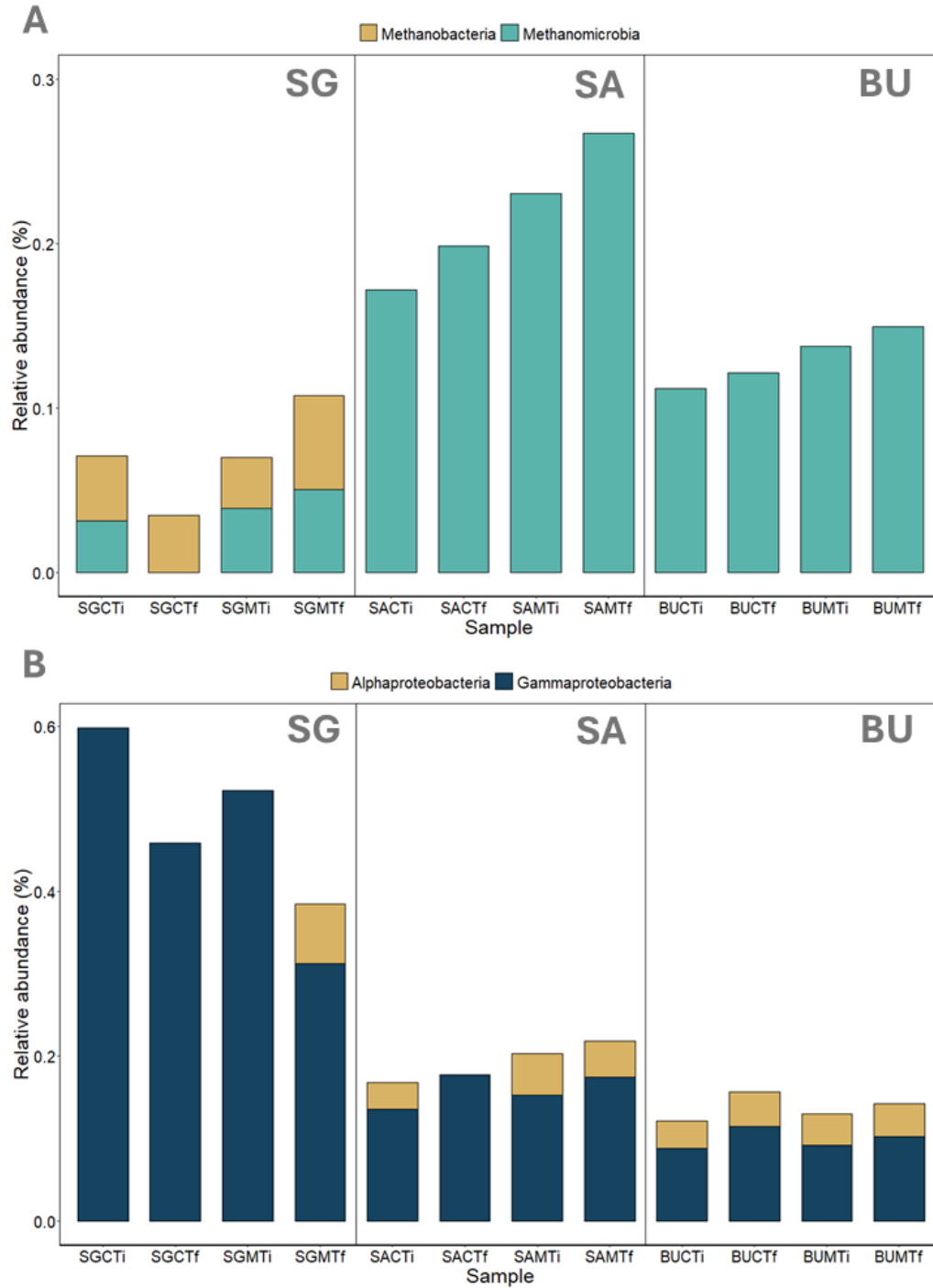


Figure S10. A) ASV relative abundance (%) of methanogenic archaea classes: Methanobacteria (yellow) and Methanomicrobia (green) for the three studied lakes (SG, SA and BU). B) ASV relative abundance (%) of methanotrophic bacteria classes: Alphaproteobacteria (yellow), and Gammaproteobacteria (blue). “C” means control – the lake -, whereas “M” means mesocosm. “Ti” corresponds to the onset of the experiments, whereas “Tf” corresponds to the final time of the experiment.

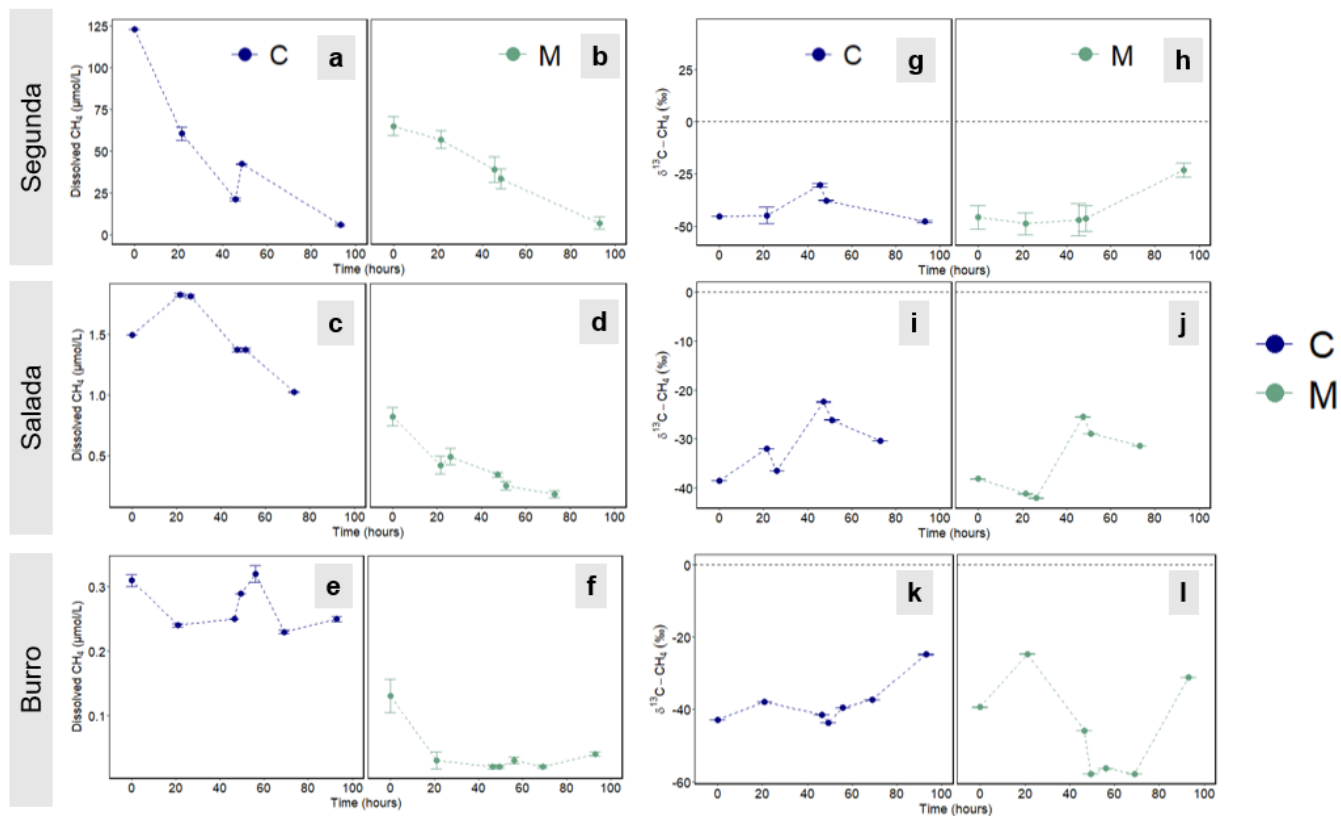


Figure S11. CH_4 dissolved (μM) and $\delta^{13}\text{C}-\text{CH}_4$ (‰) from the lake (C, Control, blue) and the mesocosms (M, green) of the lakes SG (a, b, g, h), SA (c, d, i, j) and BU (e, f, k, l). The error bars correspond to the standard deviation of all the measurements at each time point.

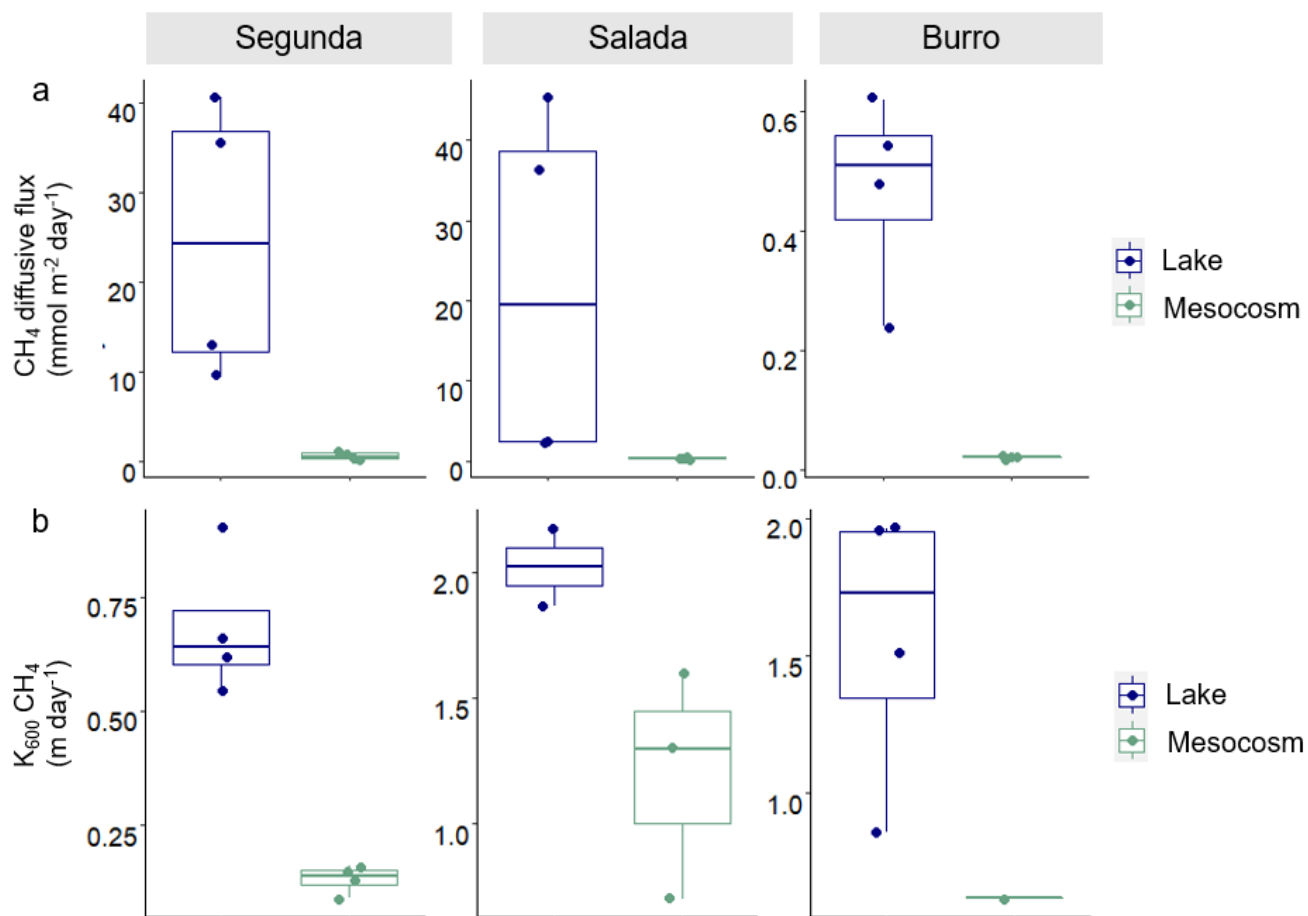


Figure S12. CH₄ diffusive flux (upper panel) and K₆₀₀ CH₄ (bottom panel) measured in the lake (blue) and in the mesocosms (green) of each one of the three studied lakes.

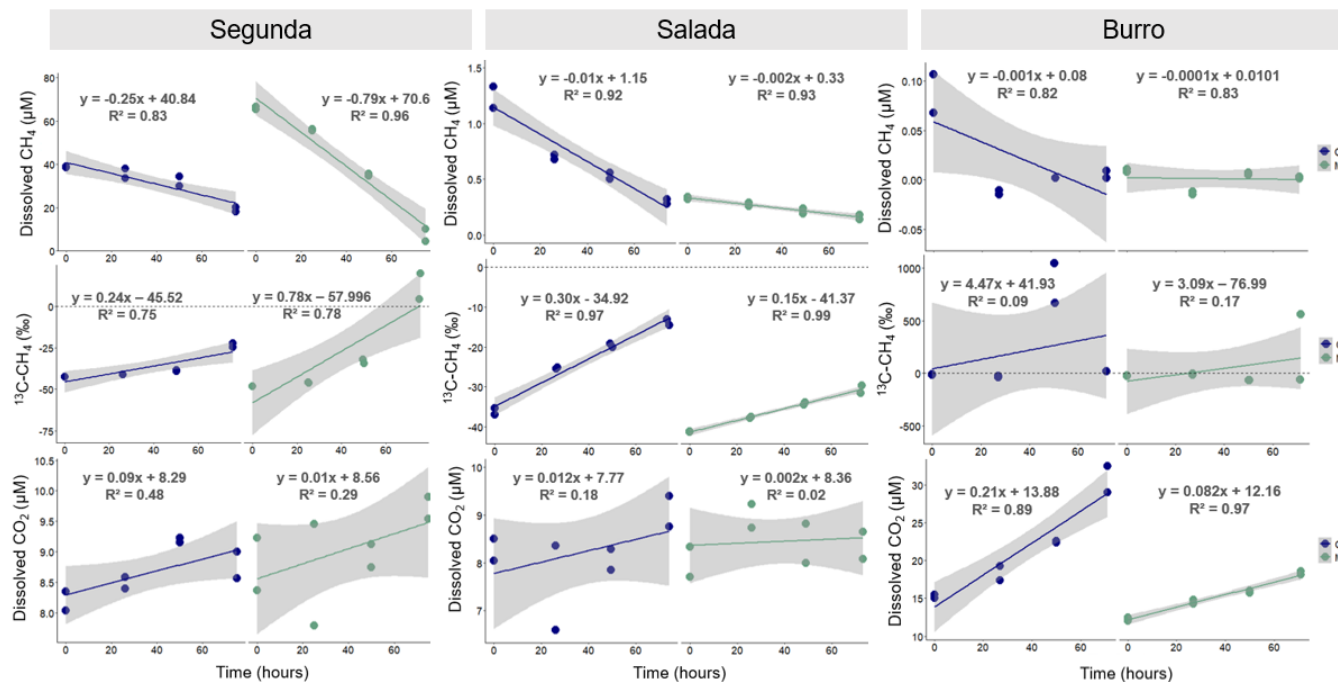


Figure S13. CH_4 dissolved (μM), $\delta^{13}\text{C}\text{-CH}_4$ (‰) and CO_2 dissolved (μM) resulted from the dark incubations carried out using water from the lake (C, control, blue) or water coming from the mesocosms (M, mesocosms, green), for each lake. The grey shadow corresponds to the standard error.

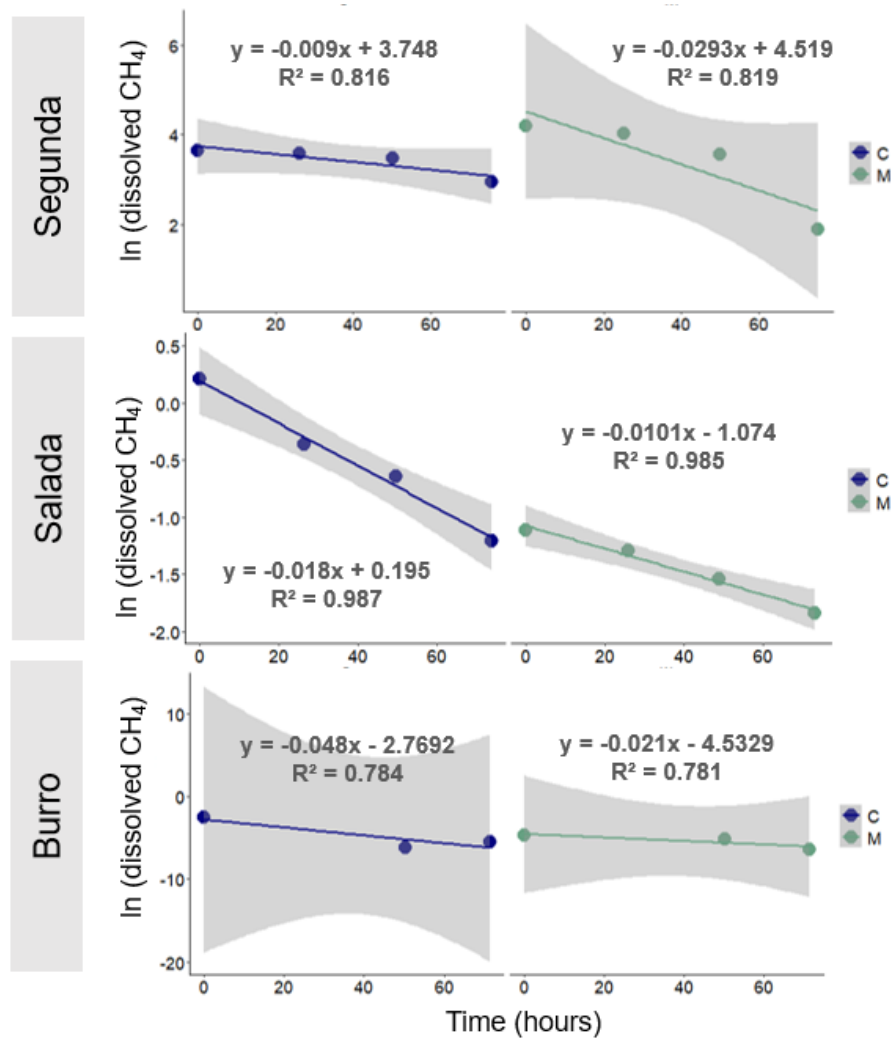


Figure S14. $\ln(\text{dissolved CH}_4)$ vs time from dark incubations, for the lake (C, control, blue) and for the mesocosms (M, mesocosms, green), and for each lake separately. The slope of this regression was used as the oxidation decay constant, K_{oxi} (hr^{-1}). The grey shadow corresponds to the standard error.

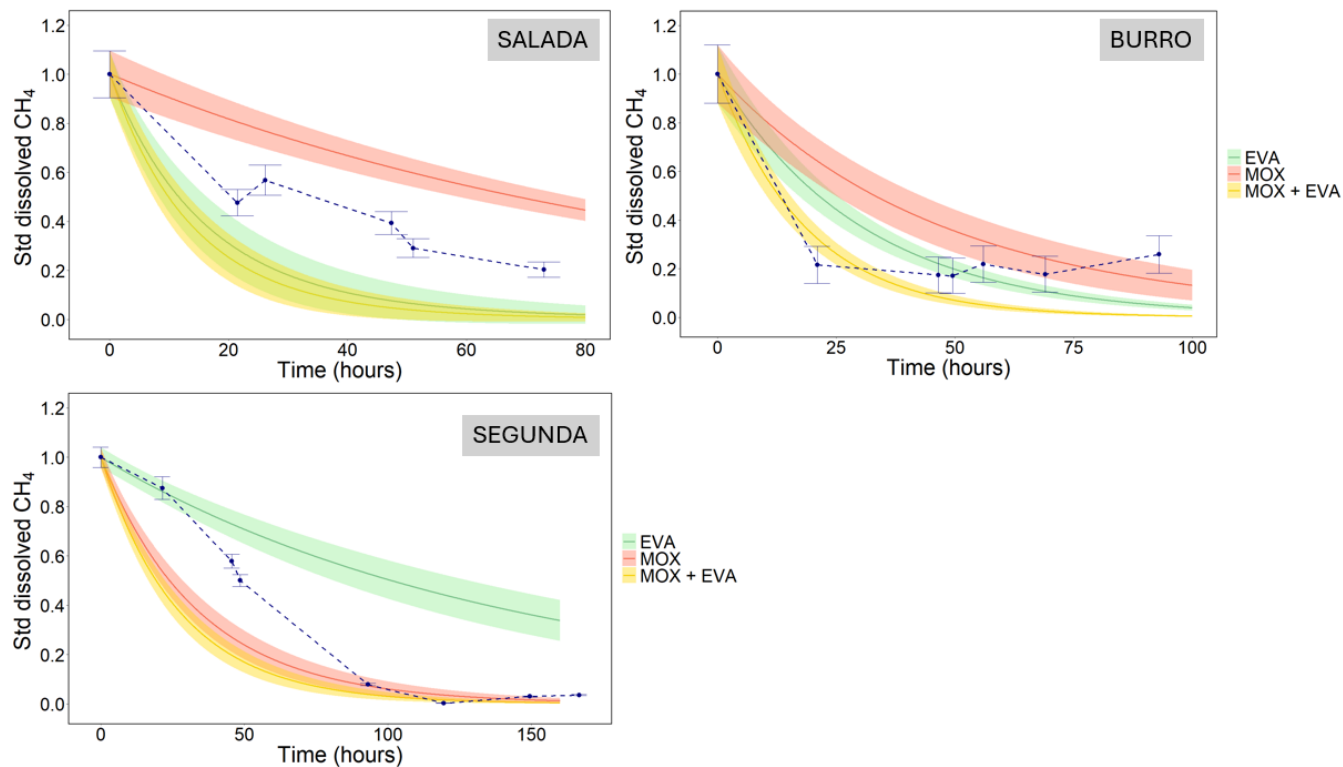


Figure S15. Expected standardized CH₄ concentrations in the mesocosms assuming only loss of methane through diffusion to the atmosphere (EVA), oxidation (MOX) or both (MOX + EVA). The shaded area around the expected curves represents the error associated with the prediction. The blue dotted line represents the observed curve.

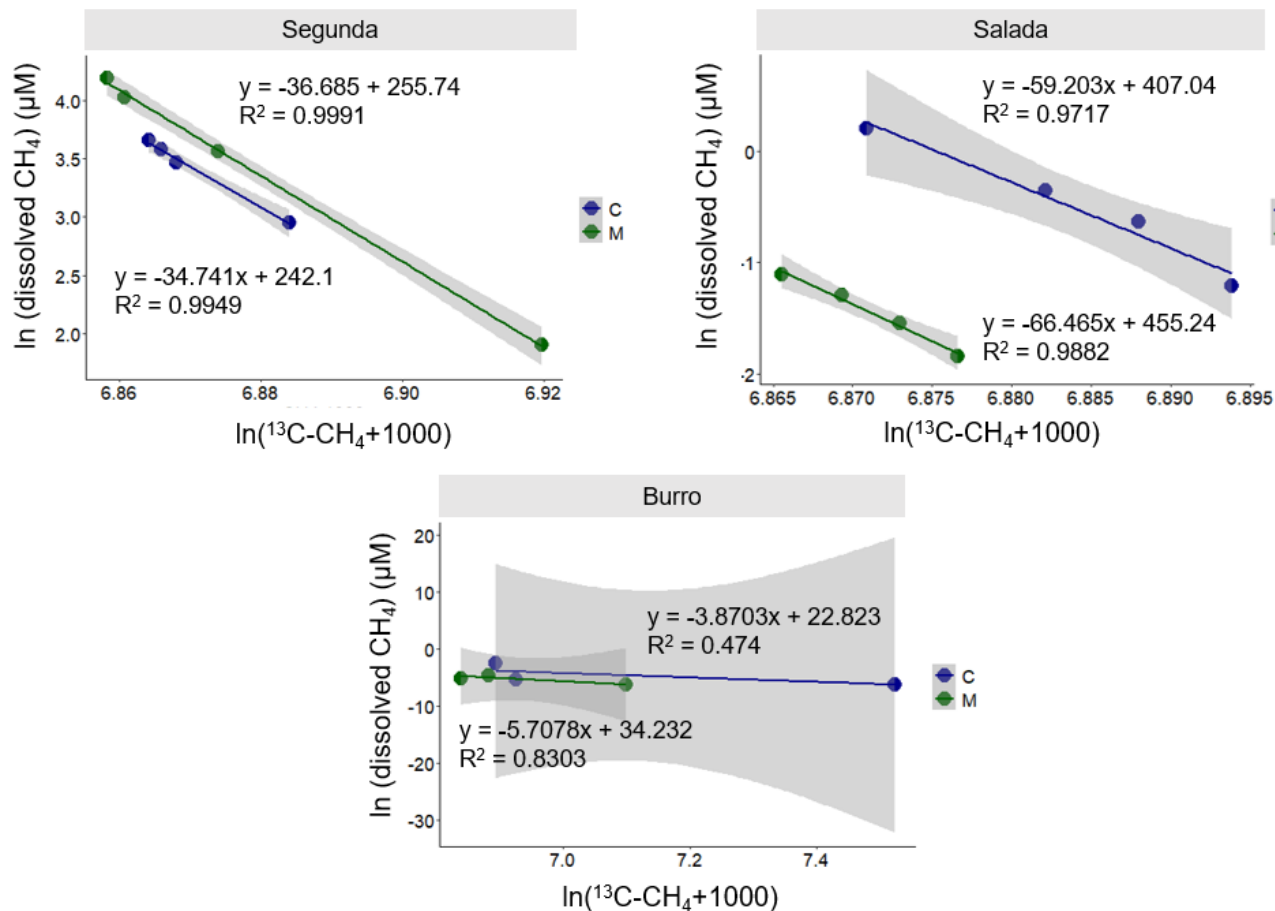


Figure S16. Linear relationship between $\ln(\text{CH}_4)$ and $\ln(\delta^{13}\text{C-CH}_4 + 1000)$ using the data from the dark incubations incubations. The slope of each regression was used to calculate the fractionation factor of oxidation (α_{oxi}) using equation 8 from the main manuscript.

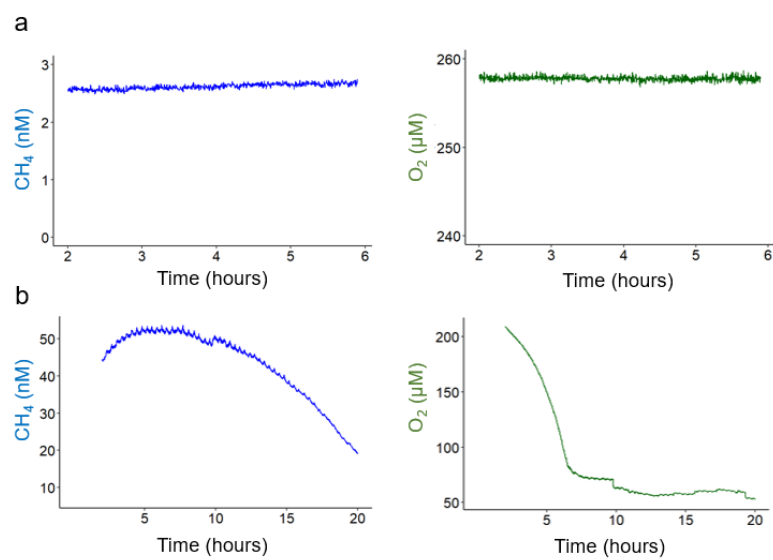


Figure S17. MIMS measurements of milliq water (a) and BG11 (b)

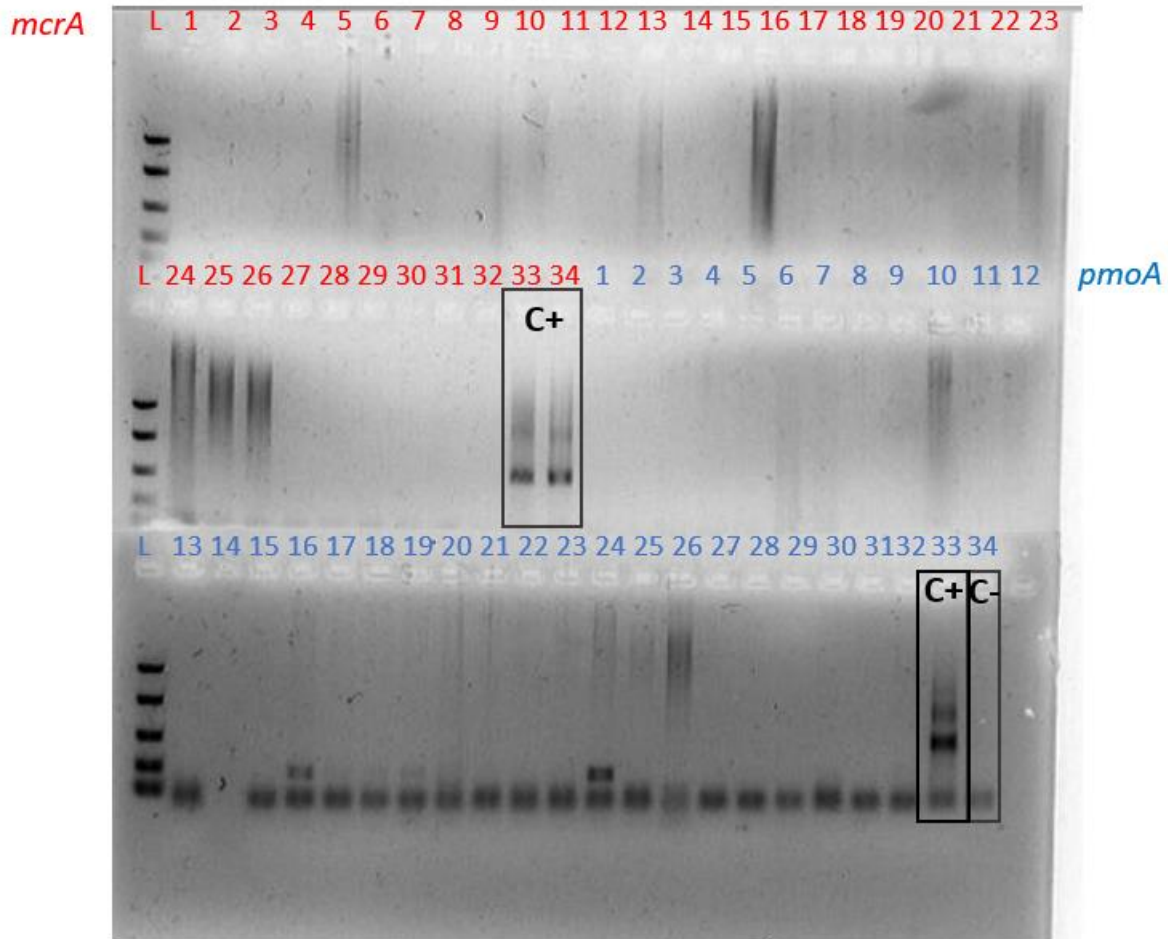


Figure S18. Agarose gel with the results of the two PCR carried out to detect methanogenic archaea (*mcrA* gene, red) and methanotrophic bacteria (*pmoA* gene, blue). In red: L stands for Ladder, streets No. 1 to No. 28 correspond to samples of *Scenedesmus linearis* (1 – 3), *Phormidium sp.* (4 – 7), *Monoraphidium sp.* (8 – 11, 27 and 28), *Scenedesmus quadricauda* (12 – 15), *Pseudanabaena sp.* (16 – 19, 24), *Leptolyngbya sp.* (20 – 23, 25 and 26), lake water extract intended as a positive control for *pmoA* that did not work (31), soil extract intended as a positive control for *mcrA* that did not work (32), positive control for *mcrA* obtained from an extract of methanogenic archaea (33 and 34). In blue: L comes from Ladder, streets No. 1 to No. 28 correspond to the same as for *mcrA*, lake water extract intended as a positive control for *pmoA* but did not work (29 and 30), soil extract intended as a positive control for *mcrA* but did not work (31 and 32), positive control for *pmoA* that worked, obtained from an extract of methanotrophic bacteria (33), and a negative control (PCR products without any culture sample, 34).

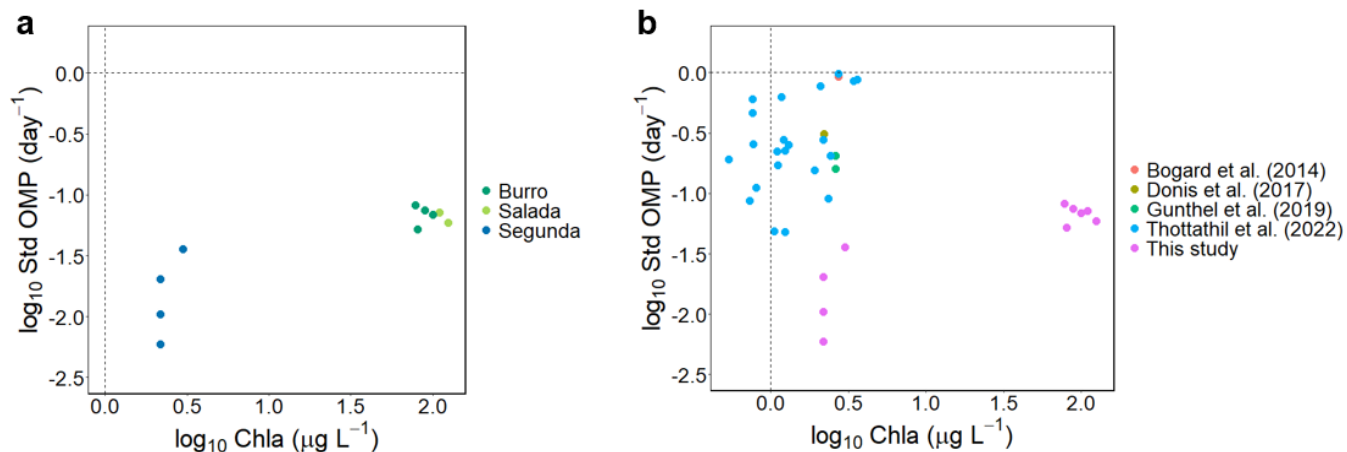


Figure S19. a) $\log_{10}(\text{standardized OMP})$ vs $\log_{10}(\text{Chla})$ including data from this study, where each color represents a lake, and b) data from this study plus other comparable studies, where each color represents a study. To estimate the standardized OMP from other studies, we divided the OMP rate in $\mu\text{M day}^{-1}$ for the mean CH_4 dissolved concentration in the lake (Donis et al., 2017; Günthel et al., 2019; Thottathil et al., 2022) or mesocosm (Bogard et al., 2014), respectively.

References

- Appling, A. P., Hall, R. O., Yackulic, C. B., & Arroita, M. (2018). Overcoming Equifinality: Leveraging Long Time Series for Stream Metabolism Estimation. *Journal of Geophysical Research: Biogeosciences*, 123(2), 624–645. <https://doi.org/10.1002/2017JG004140>
- Baliña, S., Sánchez, M. L., & del Giorgio, P. A. (2022). Physical Factors and Microbubble Formation Explain Differences in CH₄ Dynamics Between Shallow Lakes Under Alternative States. *Frontiers in Environmental Science*, 10(June), 1–11. <https://doi.org/10.3389/fenvs.2022.892339>
- Baliña, S., Sánchez, M. L., Izaguirre, I., & del Giorgio, P. A. (2022). Shallow lakes under alternative states differ in the dominant greenhouse gas emission pathways. *Limnology and Oceanography*, 68(1), 1–13. <https://doi.org/10.1002/lno.12243>
- Bogard, M. J., Del Giorgio, P. A., Boutet, L., Chaves, M. C. G., Prairie, Y. T., Merante, A., & Derry, A. M. (2014). Oxidic water column methanogenesis as a major component of aquatic CH₄ fluxes. *Nature Communications*, 5(May). <https://doi.org/10.1038/ncomms6350>
- Burlacot, A., Burlacot, F., Li-Beisson, Y., & Peltier, G. (2020). Membrane Inlet Mass Spectrometry: A Powerful Tool for Algal Research. *Frontiers in Plant Science*, 11(September), 1–15. <https://doi.org/10.3389/fpls.2020.01302>
- Callahan, B. J., McMurdie, P. J., Rosen, M. J., Han, A. W., Johnson, A. J. A., & Holmes, S. P. (2016). DADA2: High-resolution sample inference from Illumina amplicon data. *Nature Methods*, 13(7), 581–583. <https://doi.org/10.1038/nmeth.3869>
- Conrad, R. (2005). Quantification of methanogenic pathways using stable carbon isotopic signatures: A review and a proposal. *Organic Geochemistry*, 36(5), 739–752. <https://doi.org/10.1016/j.orggeochem.2004.09.006>
- DelSontro, T., Boutet, L., St-Pierre, A., del Giorgio, P. A., & Prairie, Y. T. (2016). Methane ebullition and diffusion from northern ponds and lakes regulated by the interaction between temperature and system productivity. *Limnology and Oceanography*, 61, S62–S77. <https://doi.org/10.1002/lno.10335>
- Donis, D., Flury, S., Stöckli, A., Spangenberg, J. E., Vachon, D., & McGinnis, D. F. (2017). Full-scale evaluation of methane production under oxic conditions in a mesotrophic lake. *Nature Communications*, 8(1), 1–11. <https://doi.org/10.1038/s41467-017-01648-4>
- Fernández Zenoff, V., Siñeriz, F., & Farías, M. E. (2006). Diverse responses to UV-B radiation and repair mechanisms of bacteria isolated from high-altitude aquatic environments. *Applied and Environmental Microbiology*, 72(12), 7857–7863. <https://doi.org/10.1128/AEM.01333-06>

- Günthel, M., Donis, D., Kirillin, G., Ionescu, D., Bizic, M., McGinnis, D. F., Grossart, H. P., & Tang, K. W. (2019). Contribution of oxic methane production to surface methane emission in lakes and its global importance. *Nature Communications*, 10(1), 1–10. <https://doi.org/10.1038/s41467-019-13320-0>
- Hall, R. O., & Hotchkiss, E. R. (2017). Stream Metabolism. In *Methods in Stream Ecology: Third Edition* (Vol. 2). Elsevier Inc. <https://doi.org/10.1016/B978-0-12-813047-6.00012-7>
- Lorenzen, C. J. (1967). Determination of Chlorophyll and Pheo-Pigments: Spectrophotometric Equations. *Limnology and Oceanography*, 12(2), 343–346. <https://doi.org/10.4319/lo.1967.12.2.0343>
- Nercessian, O., Noyes, E., Kalyuzhnaya, M. G., Lidstrom, M. E., & Chistoserdova, L. (2005). Bacterial populations active in metabolism of C1 compounds in the sediment of Lake Washington, a freshwater lake. *Applied and Environmental Microbiology*, 71(11), 6885–6899. <https://doi.org/10.1128/AEM.71.11.6885-6899.2005>
- Odum, H. T. (1956). Primary Production in Flowing Waters. *Limnology and Oceanography*, 1(2), 102–117. <https://doi.org/10.4319/lo.1956.1.2.0102>
- Samad, M. S., & Bertilsson, S. (2017). Seasonal variation in abundance and diversity of bacterial methanotrophs in five temperate lakes. *Frontiers in Microbiology*, 8(FEB), 1–12. <https://doi.org/10.3389/fmicb.2017.00142>
- Soued, C., & Prairie, Y. T. (2021). Changing sources and processes sustaining surface CO₂ and CH₄ fluxes along a tropical river to reservoir system. *Biogeosciences*, 18(4), 1333–1350. <https://doi.org/10.5194/bg-18-1333-2021>
- Strickland, J. D. H., & Parson, T. R. (1965). A Manual of Seawater Analysis, 2nd edit. In *A Manual of Seawater Analysis, 2nd edit*. Issued by Fisheries Research Board of Canada.
- Thottathil, S. D., Reis, P. C. J., & Prairie, Y. T. (2022). Magnitude and Drivers of Oxic Methane Production in Small Temperate Lakes. *Environmental Science and Technology*, 56(15), 11041–11050. <https://doi.org/10.1021/acs.est.2c01730>
- Wanninkhof, R. (1992). Relationship between wind speed and gas exchange over the ocean revisited. *Journal of Geophysical Research*, 12(JUN), 351–362. <https://doi.org/10.4319/lom.2014.12.351>